9
Smectic Liquid Crystals: Antiferroelectric and Ferrielectric Phases

Hideo Takezoe and Yoichi Takanishi

9.1 Introduction

New materials are discovered sometimes intentionally and sometimes accidentally. The former case can be exemplified by ferroelectric liquid crystals (FLCs), wherein the chirality was introduced into the lateral chain to reduce the symmetry, leading to a noncentrosymmetric system [1]. In the latter case, it can be referred to as antiferroelectric liquid crystals (AFLCs) which were discovered accidentally. Actually, compounds which exhibit the antiferroelectric phase had been synthesized several years before they were proven as AFLCs. The hitherto known AFLCs include three materials, as shown in Figure 9.1: (1) MHPOBC, (2) MHTAC, and (3) (*R*) and (*S*)-1-methylpentyl 4′-(4″-*n*-decyloxybenzoyloxy)bipheny-l-4-carboxylates.

MHPOBC was first reported as a new FLC in the Japan domestic liquid crystal meeting in 1985 by Inukai et al. [2]. In the First International FLC Conference in 1987, two groups pointed out unusual behavior in this compound. Hiji et al. [3] reported a third stable state exhibiting a dark view between crossed polarizers when one of the polarizers is parallel to the smectic layer. Furukawa et al. [4] reported a very small dielectric constant and a threshold behavior in the electro-optic response in the lower temperature region of SmC*, suggesting a new phase, SmY*.

The MHTAC analogue was first synthesized in 1976, and MHTAC itself appeared in the literature in 1983 [5]. However, the herring-bone (antiferroelectric) structure of this material was first reported in the Second International FLC Conference (1989, Goteborg) [6]. At the same conference, Takezoe et al. also reported the antiferroelectricity of MHPOBC [7], [8]. Goodby and Chin [9] also synthesized and reported (*R*) and (*S*)-1-methylpentyl 4′-(4″-*n*-decyloxybenzoyloxy)biphenyl-4-carboxylates in 1988 without noticing the existence of the antiferroelectric phase in these compounds.

Thus, an induction period was necessary to identify the antiferroelectric structure after the synthesis of the AFLC materials and the discovery of some characteristic features. This period was required to justify the incompatibility of the antiferroelectric structure with the molecular arrangement in

1 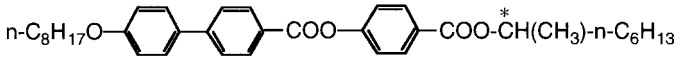

2 

3 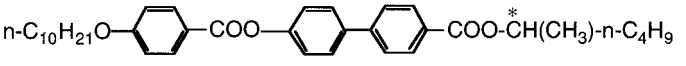

FIGURE 9.1. Chemical structures of three antiferroelectric compounds reported without realizing them as antiferroelectric ones.

liquid crystals, in which the herring-bone molecular arrangement is strongly ruled out in liquid crystals from the viewpoint of packing entropy or excluded volume effect. Actually, all the molecular arrangements in the other liquid crystalline systems composed of rod-like molecules are such that the neighboring molecules tend to be parallel to each other.

The most important observation of AFLCs was made in 1988 before the identification of the antiferroelectric phase; i.e., tristable switching with a sharp threshold and a double hysteresis [10]. The tristable switching is observable by two methods, i.e., the electro-optic effect and the switching current measurements. These results are shown in Figure 9.2 [10], in which

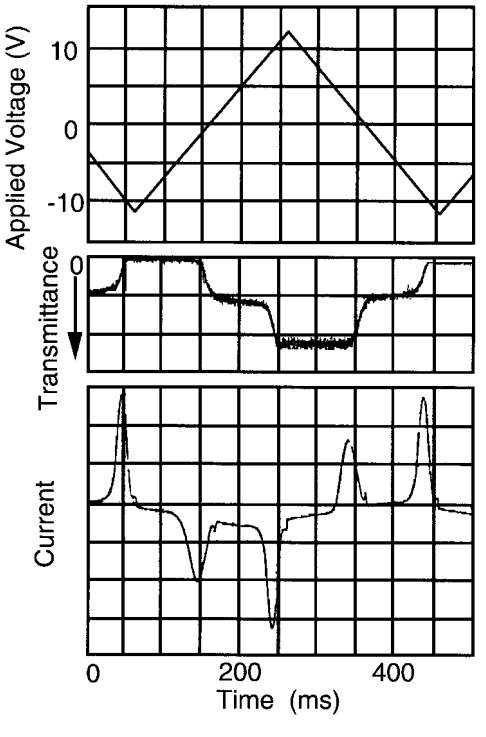

FIGURE 9.2. Transmittance change and switching current observed by applying a triangular voltage wave in MHPOBC [10]. Note that two changes in the transmittance and two peaks in the switching current are observed.

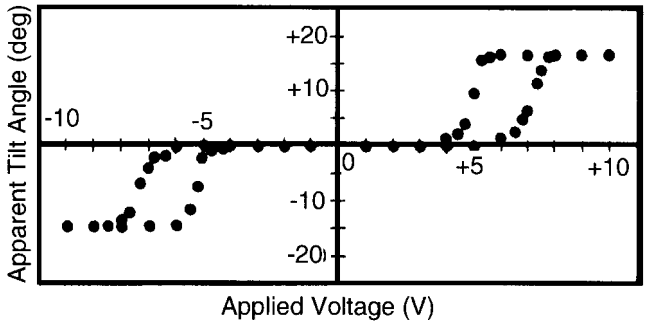

FIGURE 9.3. Apparent tilt angle under the application of a dc electric field in MHPOBC [10]. Note the threshold and double hysteresis behaviors.

two switching current peaks appear when sharp transmittance changes occur. Figure 9.3 shows the apparent tilt angle under the application of a dc electric field [10]. It is easily noticed that a switching device could be made by utilizing the threshold and the hysteresis. Figure 9.4 demonstrates the transmittance changes by applying positive and negative pulses superposed on a biased voltage [10]. This is the essential principle of the tristable AFLC display [11].

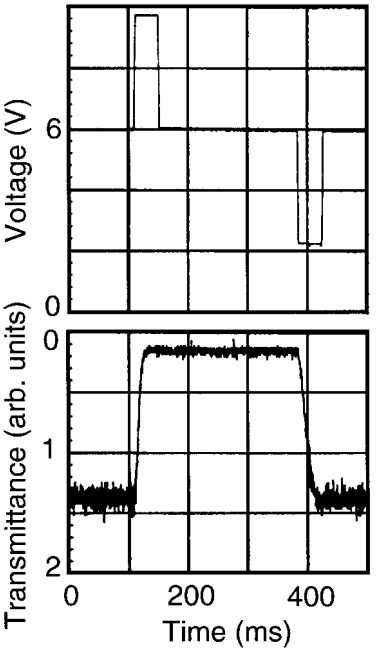

FIGURE 9.4. Electro-optic response by applying positive and negative pulses superposed on a biased voltage (6 V) in MHPOBC [10].

9.2 Experimental Observations Indicating the Antiferroelectric Structure

The helicoidal structures of FLCs and AFLCs are shown in Figures 9.5(a) and (b), respectively. In the antiferroelectric structure, the helicoidal pitch is normally of the order of 1 μm, so that several hundreds of layers exist in a pitch length. Therefore, the molecules in the neighboring layers tilt almost to the opposite directional sense. The local molecular arrangement in the AFLCs is shown in Figure 9.5(c).

At least four experimental observations, which strongly suggest or certify the antiferroelectric structure, were made. They are:

(1) transmittance spectra in oblique incidence;
(2) interferential microscope observation of a droplet;
(3) ellipsometry for free-standing films; and
(4) microscope observation of defects.

It is easy to understand the difference of the optical properties of the ferroelectric and antiferroelectric helicoidal structures shown in Figures 9.5(a) and (b). For light propagating along the helicoidal axis, the two structures are apparently the same, since half the pitch is optically one period in both structures. In contrast, for obliquely incident light, the molecular orientations

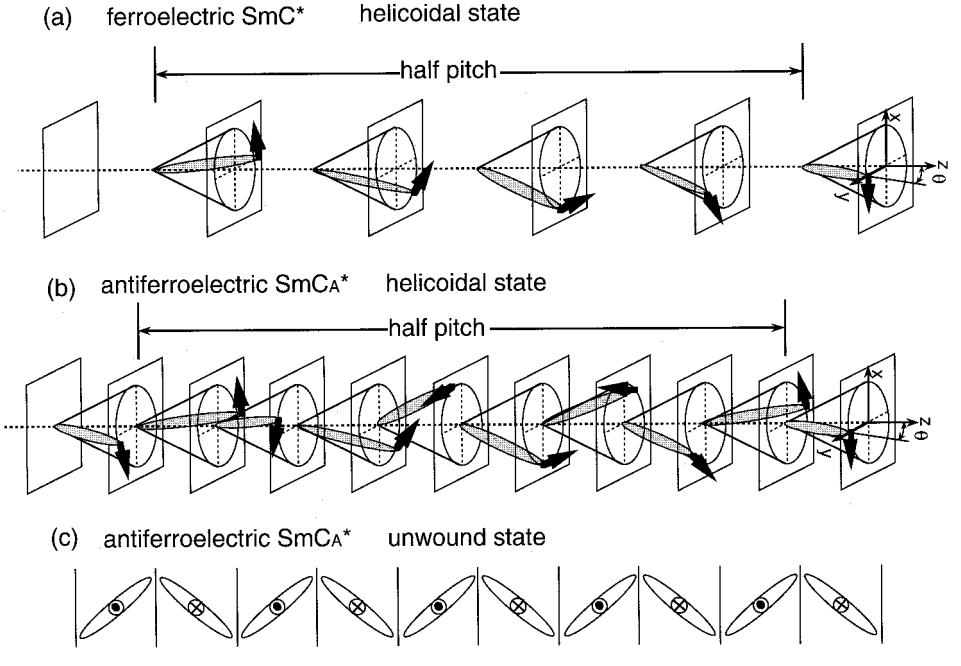

FIGURE 9.5. Helicoidal structures of the ferroelectric and antiferroelectric phases, and a local molecular arrangement in SmC_A^*.

in the layers separated by half the pitch look different, so that the optical period is a full pitch in the ferroelectric structure, while the optical period is still half the structural pitch in the antiferroelectric structure. Because of the herring-bone structure in the antiferroelectric phase, the local system is strongly biaxial and the major axis of the indecatrix is parallel to the layer normal and the two optic axes rotate about the layer normal from layer to layer due to the macroscopic helicoidal structure. Contrary to this structure, the indecatrix of the ferroelectric structure is weakly biaxial due to hindered rotation, and the major axis of the indecatrix tilts and precesses from layer to layer.

These two different structures can be easily differentiated by observing the selective reflection at oblique incidence [12]. Namely, a so-called full pitch band is observable in the ferroelectric phase at the wavelength of twice of that of the normal selective reflection band, while the full pitch band must be absent in the antiferroelectric phase. This is actually the case based on the first experimental evidence, as shown in Figure 9.6 [12], in which no full

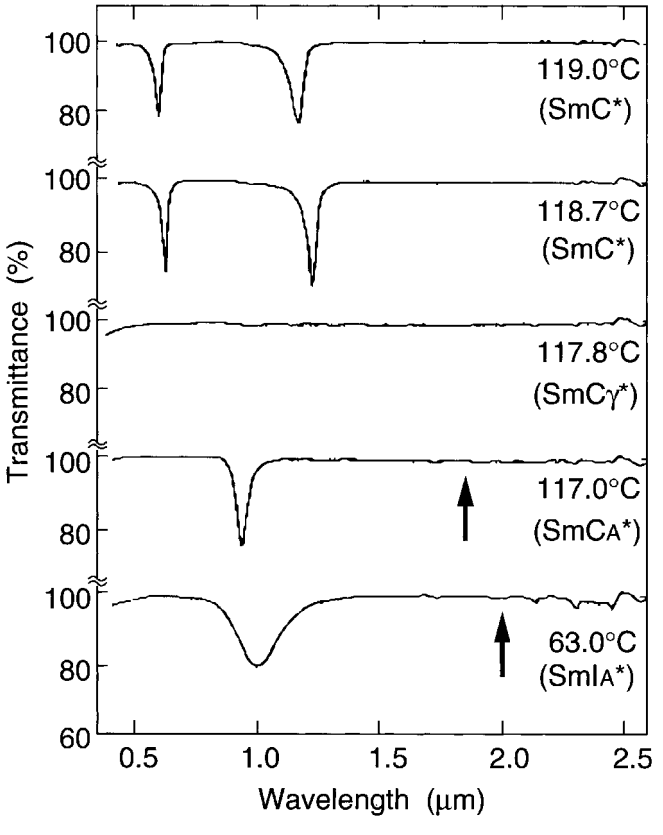

FIGURE 9.6. Transmittance spectra at oblique incidence in the ferroelectric and the antiferroelectric phases of MHPOBC [12].

pitch band can be seen at arrow positions. This presence of antiferroelectric phase can be inferred from Figure 9.6.

The herring-bone molecular arrangement in the SmO phase of MHTAC was first confirmed by an interferential microscope observation of a droplet of racemic MHTAC on a glass surface [13]. The temperature of the droplet was controlled so that a few smectic layers were formed on the isotropic droplet. By changing the temperature under the application of an electric field parallel to the glass surface, the number of layers was changed and the structure was examined. In this way, it was confirmed that the molecular tilt sense alters from layer to layer. It has been confirmed that the SmO and SmC_A phases are identical [14]–[16].

The local molecular arrangement, i.e., herring-bone structure, was also confirmed by an ellipsometry using free-standing films. The optical geometry used is shown as an inset of Figure 9.7. The phase difference $\Delta = \Delta_p - \Delta_s$ between the p and s components of the obliquely incident transmitted light was measured in free-standing films, and is shown in Figure 9.7. The phase differences under positive and negative electric fields, Δ_+ and Δ_-, are always

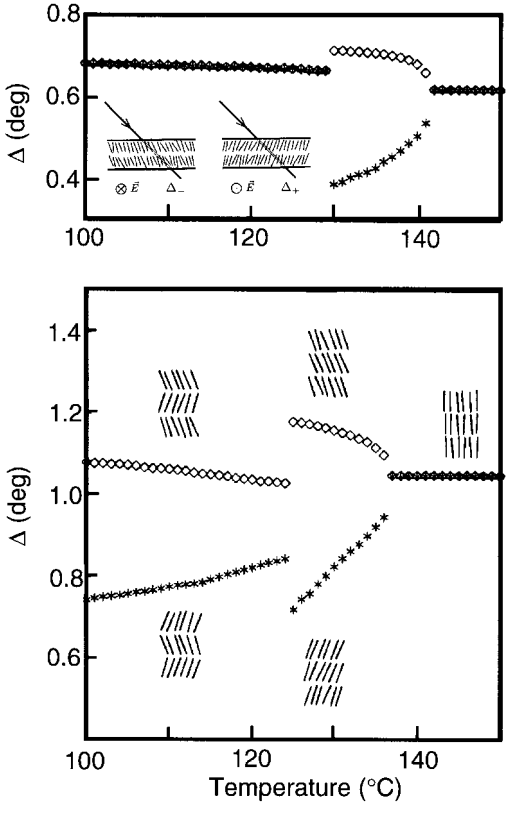

FIGURE 9.7. Phase difference between s and p components of the transmitted light measured under positive and negative fields in free-standing films [17].

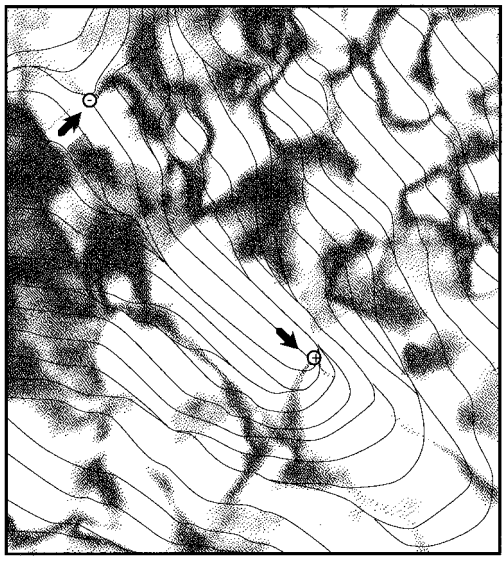

FIGURE 9.8. Schlieren texture observed in a homeotropic cell of the SmC_A phase of MHPOBC. Note the existence of two-brush defects.

different in the SmC* phase, since the molecules tilt either toward or away from the incident laser beam. In the SmC_A^* phase, however, $\Delta_+ = \Delta_-$ for two-layer films, while Δ_+ is not equal to Δ_- for three-layer films. This experiment clearly reveals the layer-by-layer alternation of the tilt and polarization direction.

To identify the antiferroelectric phase, texture observation of the homeotropic cells of racemic compounds is very effective. In the SmC phase, only the schlieren texture with four brushes is observable and that with two brushes is prohibited, because of the head-and-tail inequivalence of the C-director. In the SmC_A phase, however, the schlieren texture with two brushes is sometimes seen, as shown in Figure 9.8 [18], [19]. The existence can be explained by taking into account a screw dislocation, as illustrated in Figure 9.9. The discontinuous change (π-wall) of the C-director is compensated by the screw dislocation. This defect is a combined defect of a disclination and a dislocation, i.e., a dispiration [18], [19].

The experiments mentioned above could be used to identify the SmC_A^* phase. Other methods to identify the SmC_A^* phase are the observation of the tristable switching [10], conoscope observations [20], [21], and dielectric measurements [22], [23]. However, the tristable switching observable by the electro-optic and the switching current measurements are not enough to identify the SmC_A^* phase. Actually it was shown that FLCs with a very short pitch are possible to exhibit the tristable switching, since helicoidal structure is extremely stabilized against an applied electric field (helicoid stabilized FLCs) [24].

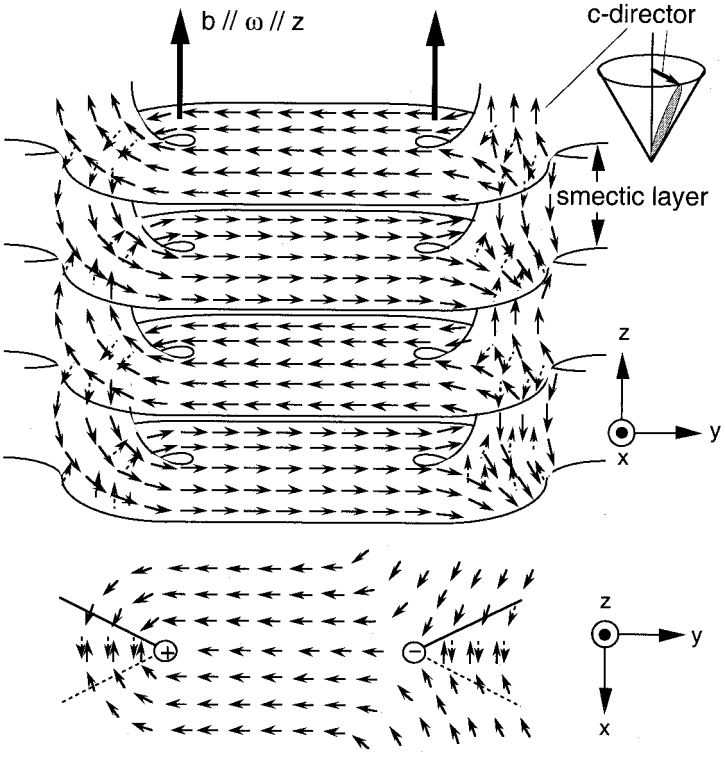

FIGURE 9.9. Model structure of the two-brush defect; i.e., dispiration, a combined defect of a wedge disclination and a screw dislocation.

9.3 Microscopic Origin of Antiferroelectricity

Generally, molecules tend to align parallel to each other in liquid crystalline phases. Therefore, we ought to seek some particular causes for the appearance of the SmC_A^* phase. The preliminary experimental observations made in this phase are summarized as follows:

(1) The SmC_A^* phase exists in compounds, the optical isomer of which have large spontaneous polarization [25].
(2) The SmC_A phase exists even in racemic compounds which have no spontaneous polarization [26]–[30].
(3) There exist compounds which show SmC* and SmC_A^* depending on chiral end chain length; odd–even behavior in the appearance of the SmC_A^* phase [28], [31].

The origin of the formation of the antiferroelectric structure has not yet been clarified. The existing ideas comprise of a dipole pairing model [32], a

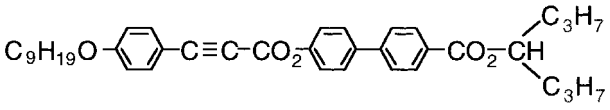

FIGURE 9.10. Chemical structure of a swallow-tailed liquid crystal compound.

P_x model [33], and a steric interaction model [34]. The importance of a steric interaction between the end chains of molecules in adjacent layers is suggested particularly, because even nonchiral molecules with swallow-tailed end chains of the same length (Figure 9.10) exhibit the antiferroelectric, more strictly anticlinic, molecular orientation [34]. The experimental observation (3) also suggests the importance of the steric interaction. Figure 9.11 shows the phase behavior in three homologous series of smetogens [31]. TFMHPOBC (see Figure 9.18) homologues have a strong tendency of antiferroelectricity and exhibit only the SmC_A^* phase. However, MHPOBC homologues and fluorine-substituted TFMHPOBC homologues show the odd–even effect.

The experimental observation (1) indicates the importance of an electric interaction. The phase behavior in the dimer liquid crystal shown in Figure 9.12 [35], [36] is very suggestive. This type of liquid crystal with an alkylene spacer is known to exhibit the conformation shown in Figure 9.13 [37]; two mesogenic groups are parallel to each other when the number of carbons of the spacer group, m, is even, while they take an anticlinic orientation for odd m. In the liquid–crystal homologues shown in Figure 9.12, this is actually the case for m less than 9, i.e., the phase sequences are Iso–SmA–SmC* for even m and Iso–SmC_A^* for odd m. However, for $m = 10$ and 12, the phase sequence Iso–SmA–SmC_A^* is realized even for even m [35]. This result can be attributed to an electric interaction stabilizing the antiferroelectric structure, which overcomes the regularity due to the conformation, by increasing the flexibility of the spacer group.

The dipole pairing model is based on the pair formation of molecules in adjacent layers through the dipole–dipole interaction. Because of the experimental observation (2), pairing must be made between like enantiomers, as shown in Figure 9.14 [32]. Otherwise, anticlinic orientation cannot be formed in the racemic compounds. Therefore, in this model, chiral molecular recognition is required. The pairing may be dynamic and may occur in optically resolved local enantiomeric domains.

The so-called P_x model is related to the polarizations existing at layer boundaries. The SmC_A^* phase has D_2 symmetry with two C_2-axes; i.e., one at the middle of the layer and perpendicular to the molecular tilt plane (P_y) and one at the layer boundary parallel to the tilt plane (P_x), as shown in Figure 9.15. Then, P_x–P_x interaction between two adjacent layer boundaries stabilizes the antiferroelectric structure, if the fluctuation of P_x is involved. Even in racemic compounds, P_x always exists, though P_y is zero. Thus, this model

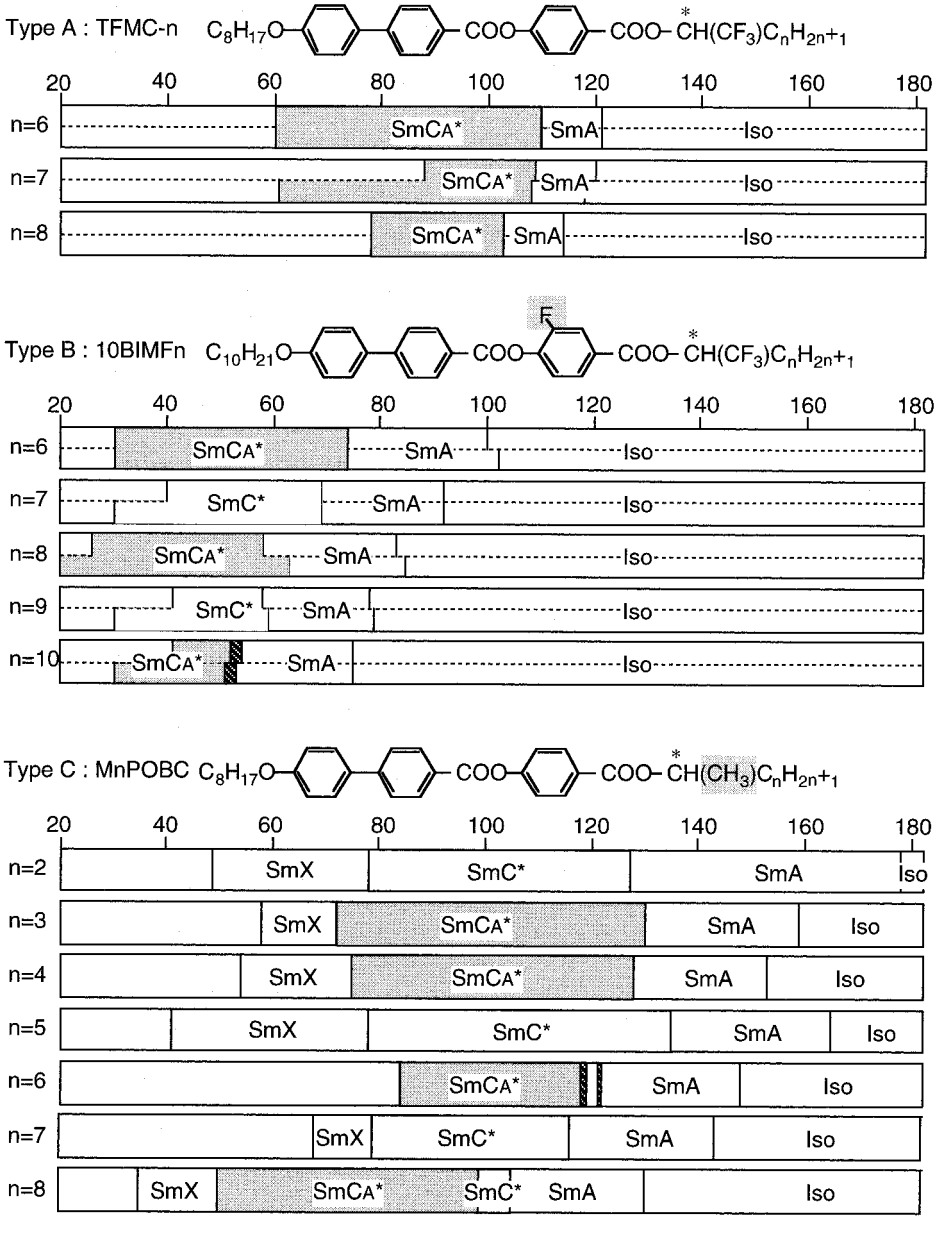

FIGURE 9.11. Phase behavior of the three homologous series of antiferroelectric liquid crystals.

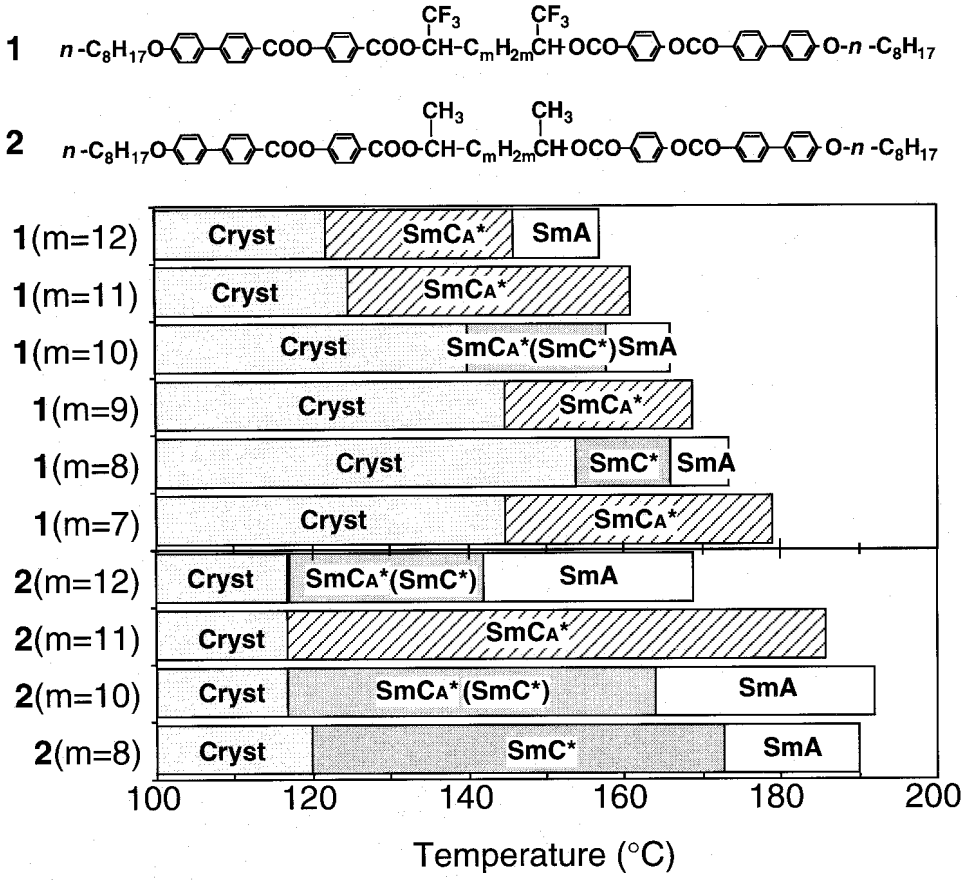

FIGURE 9.12. Chemical structures and phase sequences of dimer liquid crystal com-

satisfies the experimental observation (2). Actually, polarized FT–IR absorption of the carbonyl group (C=O) gives different polarization characteristics in SmC* and SmC_A^*, leading to different orientation of C=O, i.e., it rather lies on the tilt plane in SmC_A^* while it takes a considerably upright position in SmC* [33]. The analysis was made without taking account the different degrees of hindrance of the molecular motion about its long axis in the two phases. However, P_x always does exist irrespective of the C=O direction from the symmetry viewpoint and has an influence on the stabilization of the antiferroelectric phase.

At this moment, it is still an open question as to which of the pairings or P_x interactions plays a dominant role in stabilizing the antiferroelectric phase. In any event, for these electrostatic models to be effective, it is required that the dipoles in adjacent layers must be sufficiently close to each other. The

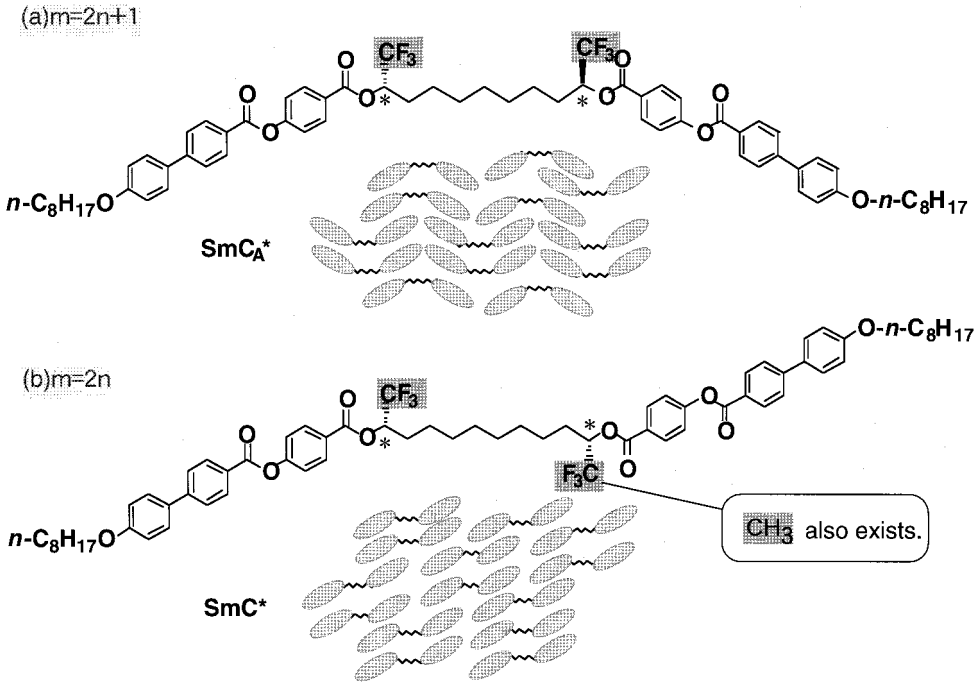

FIGURE 9.13. Two possible orientations of two mesogenic groups of the dimer liquid crystals.

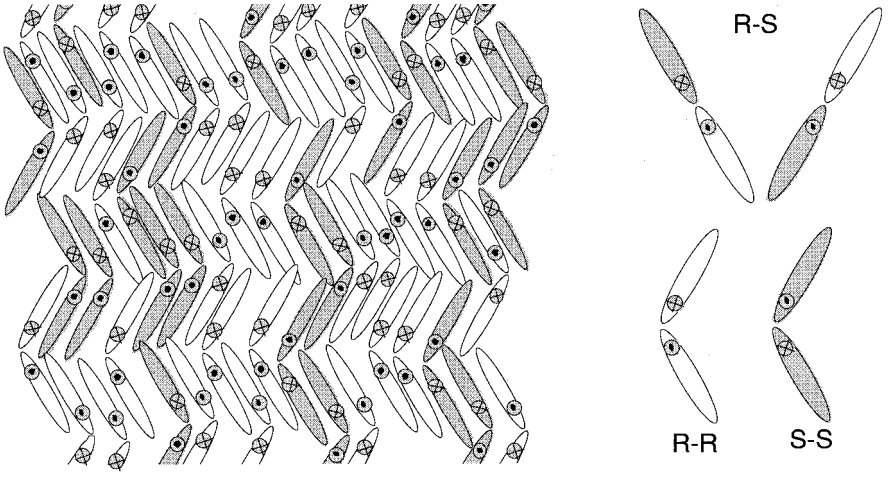

FIGURE 9.14. Possible situation of dipole pairing in a partially racemized antiferroelectric liquid crystal. Only like enantiomers make pairs.

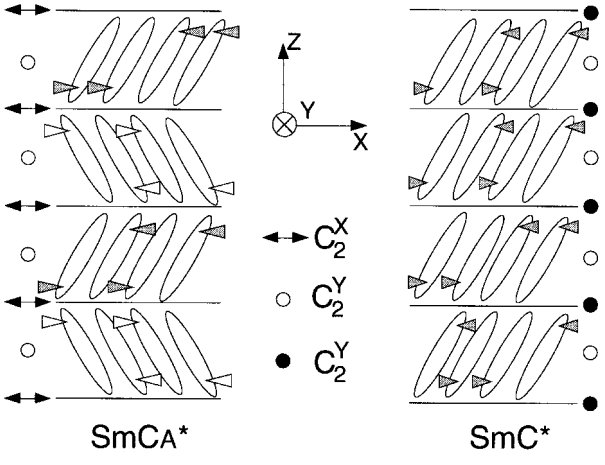

FIGURE 9.15. Two kinds of C_2-axes, along which polarization can arise; i.e., parallel and perpendicular to the tilt plane.

dipole moment responsible for the spontaneous polarization locates near the chiral center. Therefore, if the shape of the molecules is more or less straight or of a zig-zag shape, the distance between dipoles in adjacent layers will be more than 10 Å, leading to less effective dipole–dipole interaction.

The situation would be different if molecules were bent at the chiral position. The bent molecular configuration was actually confirmed in the crystalline phase of MHPOBC by X-ray diffraction [38], [39]; the chiral end chain is bent by about 90° with respect to the core direction. It was also confirmed, at least by three experiments, that the molecules are also bent even in the liquid crystalline phase. According to NMR [40], [41] and polarized FT–IR [42] measurements, the chiral chain is bent at least by the magic angle (54.7°) with respect to the core. The layer spacing of MHPOBC analogues, in which the CH_3 group at the chiral group is substituted by C_rH_{2r+1} ($r = 2 \sim 6$), increases with increasing r, suggesting the bent molecular configuration shown in Figure 9.16 [43]. Finally, the postulated molecular configuration is shown in Figure 9.17. Nevertheless, it is still necessary to confirm whether most of the antiferroelectric molecules are bent or not and whether the molecules showing only the ferroelectric phase are bent or not.

9.4 Ferrielectric and Antiferroelectric Subphases

9.4.1 Experimental Observation of Subphases

One of the most striking features of AFLCs is the emergence of various subphases. The discovery of the subphases was associated with the discovery

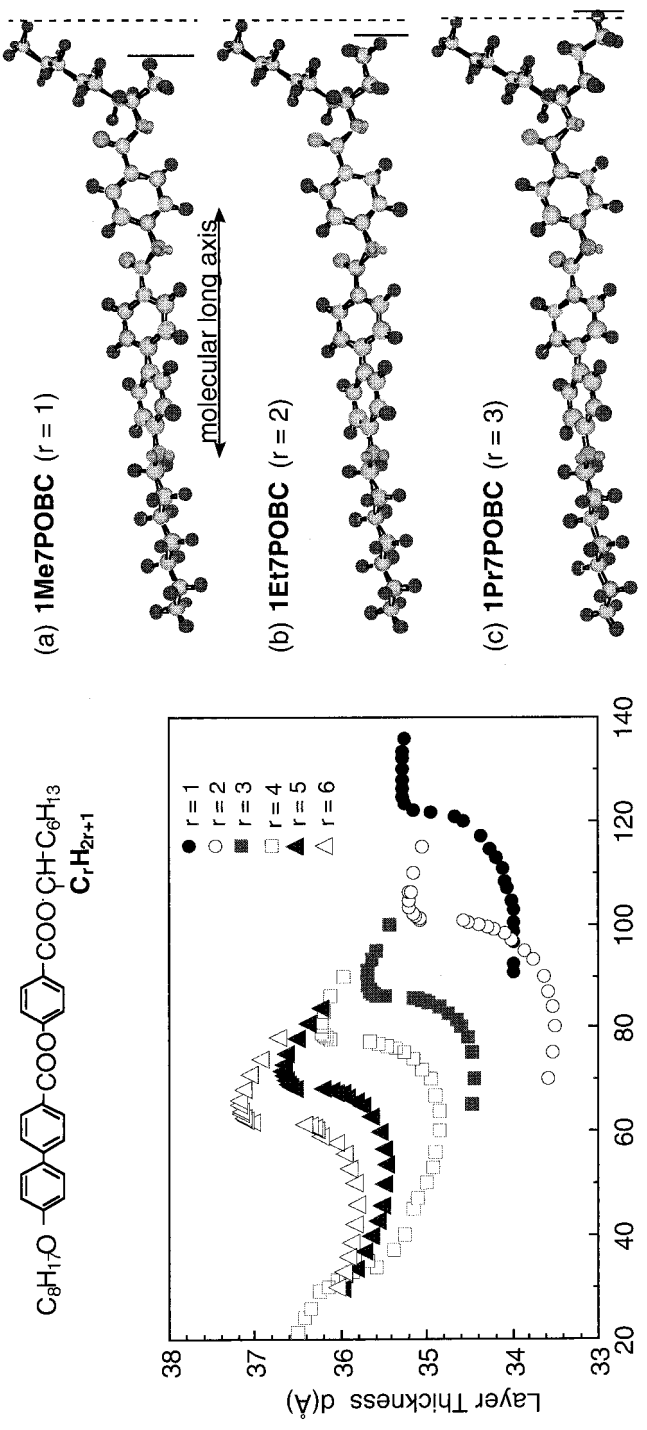

FIGURE 9.16. Temperature-dependence of the layer spacing of a homologous series of MHPOBC derivatives in which the CH_3 group at the chiral position is substituted by C_rH_{2r+1} ($r = 2 \sim 6$) [43]. The molecular structures obtained by MOPAC are also shown.

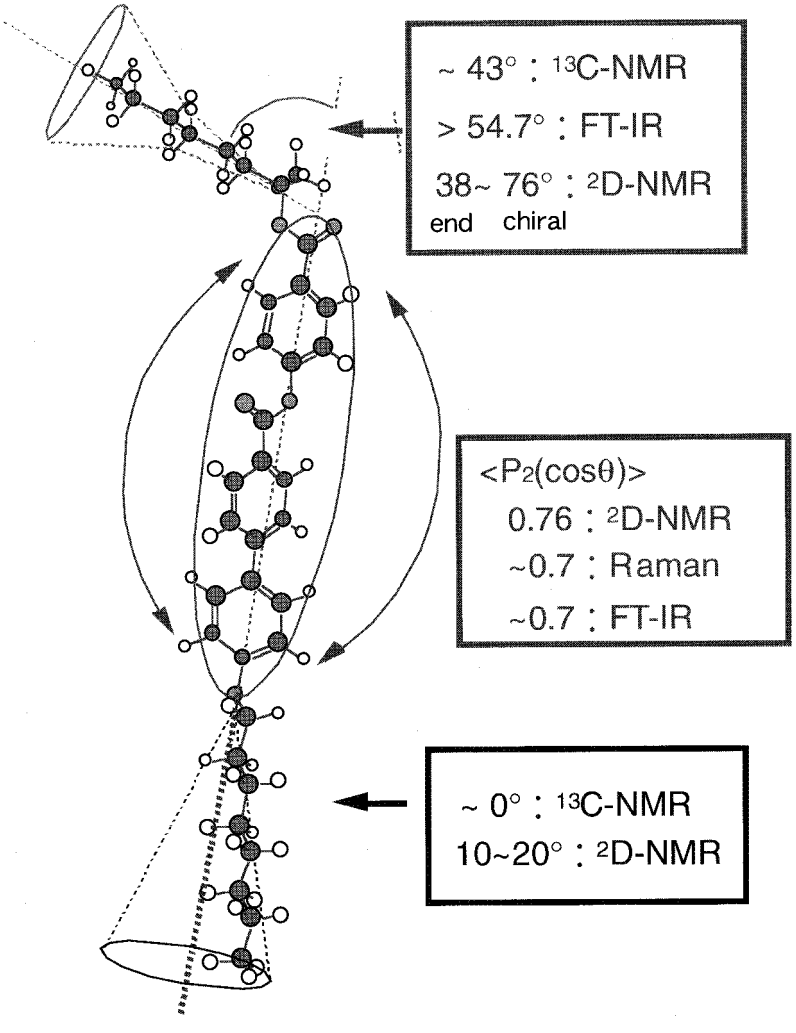

FIGURE 9.17. Molecular configuration of MHPOBC in SmA suggested by NMR, FT–IR, and X-ray analysis.

of the antiferroelectric phase in MHPOBC, which exhibits the SmCα^* phase between SmA and SmC* and the SmCγ^* phase between SmC* and SmC$_A^*$ [12]. Later a reentrant antiferroelectric phase, called the AF phase, was discovered in MHPBC (see Figure 9.18) between SmCα^* and SmCγ^* [44].

Ferroelectric and antiferroelectric compounds possessing a similar core structure are summarized in Figure 9.18. These compounds are arranged almost in order of the strength of their ferroelectricity. Namely upper and

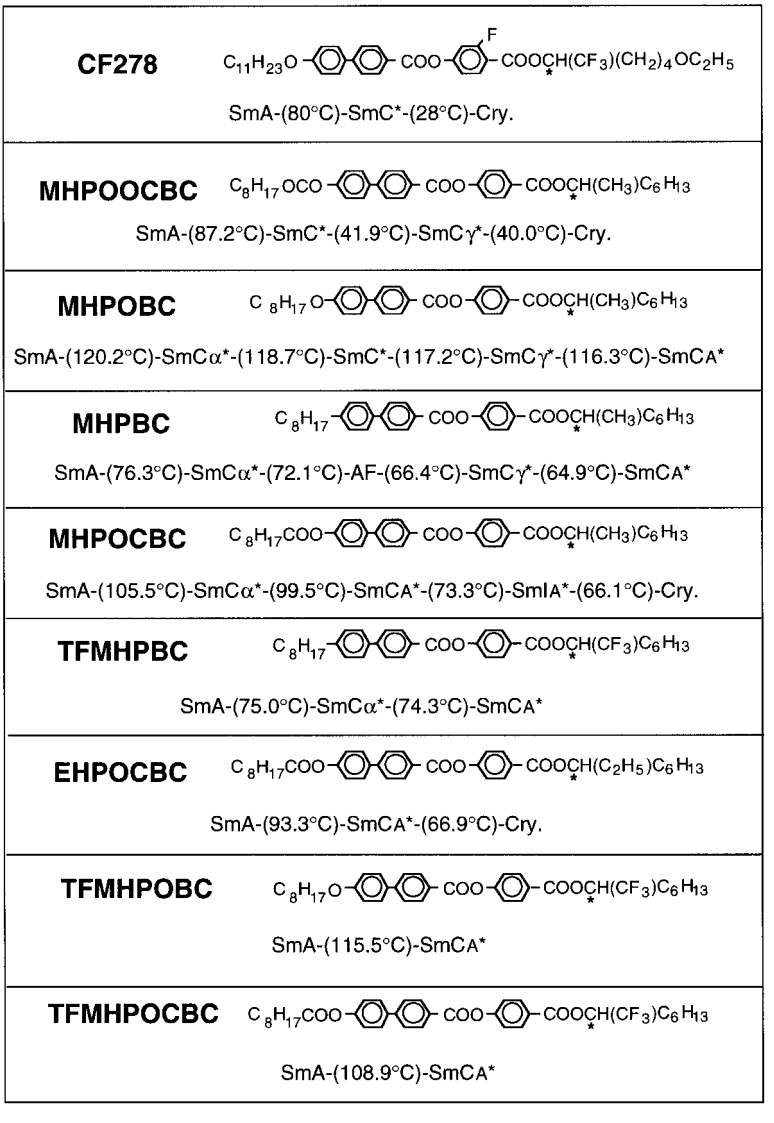

FIGURE 9.18. Ferroelectric and antiferroelectric compounds with a similar core structure.

lower compounds have stronger ferroelectricity and antiferroelectricity, respectively, and exhibit only the ferroelectric and antiferroelectric phases, respectively. In MHPOOCBC, SmC_A^* is hidden by crystallization and only the subphase $SmC\gamma^*$ appears. Moreover, the temperature range of SmC* is fairly wide. Thus, MHPOOCBC has relatively high ferroelectricity and weak

antiferroelectricity. In MHPBC, on the other hand, the SmCα^* and AF phases appear in addition to SmCγ^*, and SmC* disappears, indicating that this material has relatively high antiferroelectricity. When the antiferroelectricity becomes more intense, subphases except for SmCα^* disappear (MHPOCBC and TFMHPBC) and finally all the subphases disappear and the direct transition from SmA to SmC_A^* occurs (EHPOCBC, TFMHPOBC, and TFMHPOCBC).

The phase transitions can be identified by many techniques such as a thermal measurement [45]–[48], microscope observation, a dielectric measurement [22], and a layer spacing measurement by X-ray diffraction [31]. A much advanced technique such as ellipsometry [17] and the observation of freely suspended films under temperature gradient [49] could also be utilized. However, the identification of these subphases is not easy. Isozaki et al. [50]–[53] have adopted mainly conoscopic observations using homeotropic cells or freely suspended films [20], [21]. The conoscopic figures in all the phases exhibit a uniaxial pattern in the absence of an electric field, although the center of the extinction cross is not completely dark because of the rotatory power due to helicoidal structures. Therefore, the conoscopic observations to identify phases must be made under an electric field. Figure 9.19 shows typical conoscopic figures in the SmCα^*, SmC*, SmCγ^*, and SmC_A^* phases under an appropriate electric field. All of them exhibit biaxial figures characteristic of the respective phases.

The richness of subphases is recognized by mixing two compounds. The richness is enhanced when two compounds have moderate strength of antiferroelectricity and ferroelectricity. In order to make phase diagrams of binary mixtures, phase diagrams of temperature versus electric field (T–E phase diagram) have to be made for several binary mixtures. An example is shown in Figure 9.20, in which the mixtures of two compounds (EHPOCBC and MHPOOCBC) were used [51]. Using these T–E phase diagrams, the phase diagram of temperature versus wt% (x) of EHPOBC (T–x phase diagram) is drawn, as shown in Figure 9.21(a) [51]. Other T–x phase diagrams in Figure 9.21 are for some other binary mixtures [50], [51], [53]. In this way, at least five subphases have been suggested to appear between SmC* and SmC_A^*; i.e., SmC*–FI–AF–FI_H–SmCγ^*–FI_L–SmC_A^* even though they are not always observable. However, if they exist, they do appear with the same order.

The T–x phase diagrams of isomers with various optical purities are also shown in Figure 9.22 [52]. At first, it was thought that the SmCα^* phase exists only in enantiomers with high optical purity [26], [46], as shown in Figures 9.22(a) and (b); and the SmC* phase is injected or becomes wider with decreasing optical purity, as shown in Figures 9.22(a) and (c). However, SmCα^* is injected by lowering the optical purity in TFMHPOCBC (Figure 9.22(d)) and SmC* is not injected even in racemate (Figure 9.22(b)). All the phase behavior could be interpreted by taking into account the competing interaction of ferroelectricity and antiferroelectricity [54].

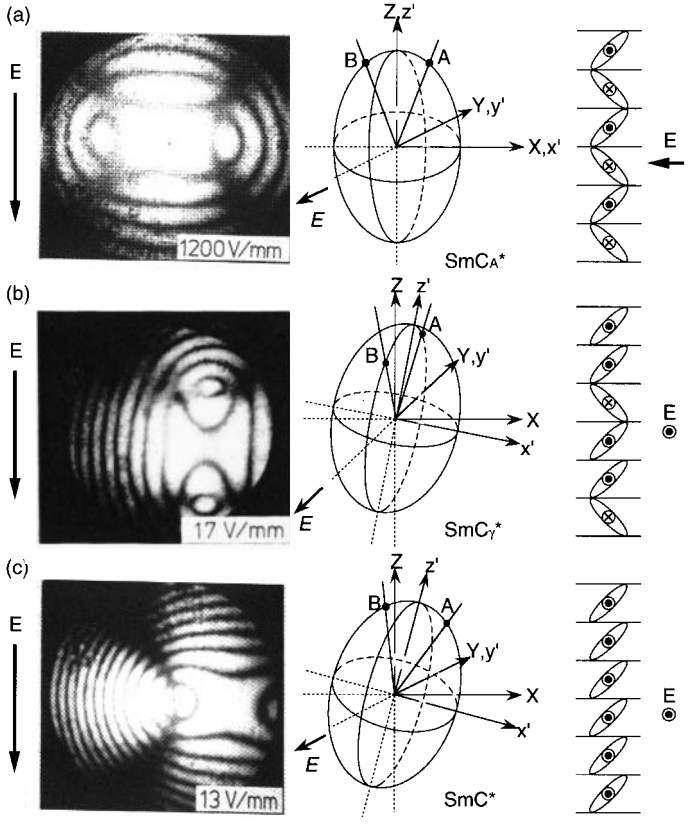

FIGURE 9.19. Typical conoscopic figures, indices of ellipsoid, and molecular arrangements in the SmC_A^*, $SmC\gamma^*$, and SmC* phases under appropriate electric fields.

9.4.2 *Theoretical Treatment*

The theoretical treatment for explaining the structures of the subphases is classified into two, i.e., the Ising model and XY model. In the Ising model, molecules locally lay on a plane and tilt right or left, while they distribute at any azimuthal angles on a cone in the XY model. From the above discussion, it is evident that there exist competing interactions which stabilize ferroelectricity and antiferroelectricity; i.e., the excluded volume effect stabilizes a ferroelectric (synclinic) structure and the dipole–dipole interaction or steric interaction stabilizes an antiferroelectric (anticlinic) structure. We discussed the appearance of various subphases based on the one-dimensional Ising model with long-range repulsive interactions developed by Bak and Bruinsma [55], [56]. Namely, because of the competing interaction of

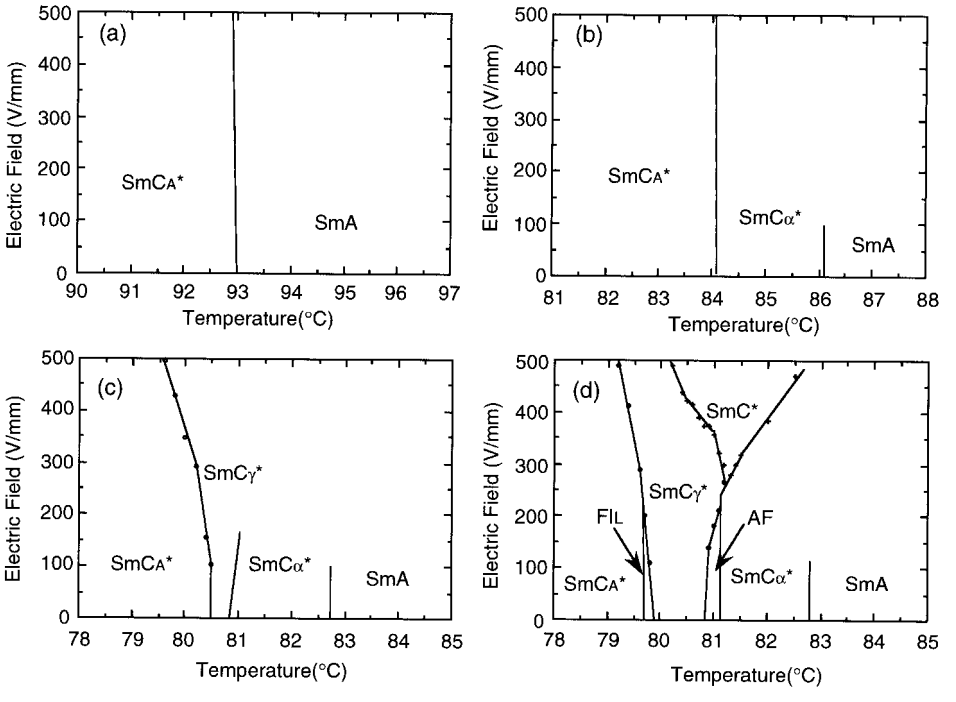

FIGURE 9.20. T–E phase diagrams of binary mixtures of EHPOCBC and MHPOOCBC with various mixing ratios: (a) (R)-EHPOCBC; (b) 50.0% (R)-EHPOCBC in (R)-MHPOOCBC; (c) 19.8% (R)-EHPOCBC in (R)-MHPOOCBC; and (d) 18.8% (R)-EHPOCBC in (R)-MHPOOCBC.

ferroelectricity and antiferroelectricity, ferroelectric (F) ordering is excited in antiferroelectric (A) ordering and the ferroelectrically ordered positions distribute uniformly due to a long-range repulsion interaction between the F orderings [54]. Since the fraction of F ordering is possible for every rational number q, an infinite number of subphases may appear, the devil's staircase [57]. According to this model, the major subphases, SmCγ^* and AF, are described by the structures shown in Figure 9.23.

Yamashita and Miyazima [58] and Yamashita [59], [60] adopted the modified ANNNI (axial next-nearest-neighbor Ising) model with the third-neighboring interaction (ANNNI + J_3 model) and wrote the Hamiltonian

$$H = -J\sum_{(i,j)} s_i s_j - J_1 \sum_i s_i s_{i+1} - J_2 \sum_i s_i s_{i+2} - J_3 \sum_i s_i s_{i+3}, \qquad (9.1)$$

where the Ising spin s_i takes a value of ± 1 corresponding to the molecular tilting senses of the ith smectic layer. The first summation is taken over nearest-neighboring pairs (i, j) in the same smectic layer, and other summa-

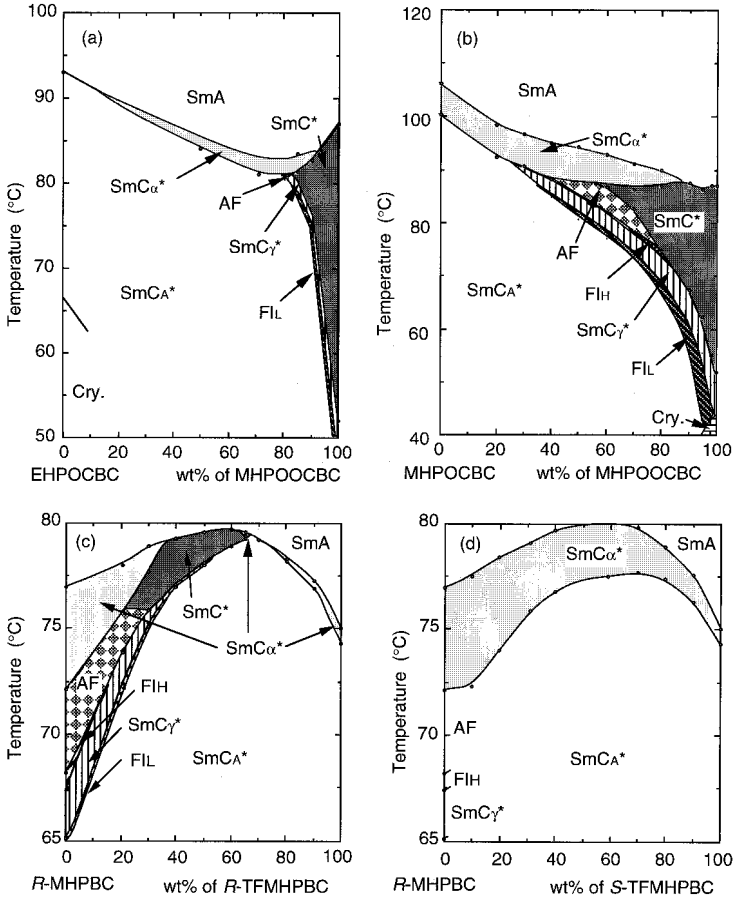

FIGURE 9.21. T–x phase diagrams of: (a) (R)-EHPOCBC and (R)-MHPOOCBC; (b) (R)-MHPOCBC and (R)-MHPOOCBC; (c) (R)-MHPBC and (R)-TFMHPBC; and (d) (R)-MHPBC and (S)-TFMHPBC.

tions are only for the first, second, and third neighboring pairs in the axial direction parallel to the layer normal; the second-nearest-neighbor interaction J_2 should be negative to ensure competition, and the third-nearest-neighbor interaction J_3, which is positive or negative, is included for the possible wide stability of SmCγ^*. Yamashita [61], [62] also pointed out an important role played by the directional sense of the molecular long axis and gave realistic physical grounds for these rather long-range interactions. A similar treatment has been adopted by Koda and Kimura [63].

Yamashita showed that four ground states appear, i.e., $\mathrm{SmC}_\mathrm{A}^*$ ($q = \frac{1}{2}$), SmCγ^* ($q = \frac{1}{3}$), AF ($q = \frac{1}{4}$), and SmC* ($q = 0$), as illustrated in Figure 9.24.

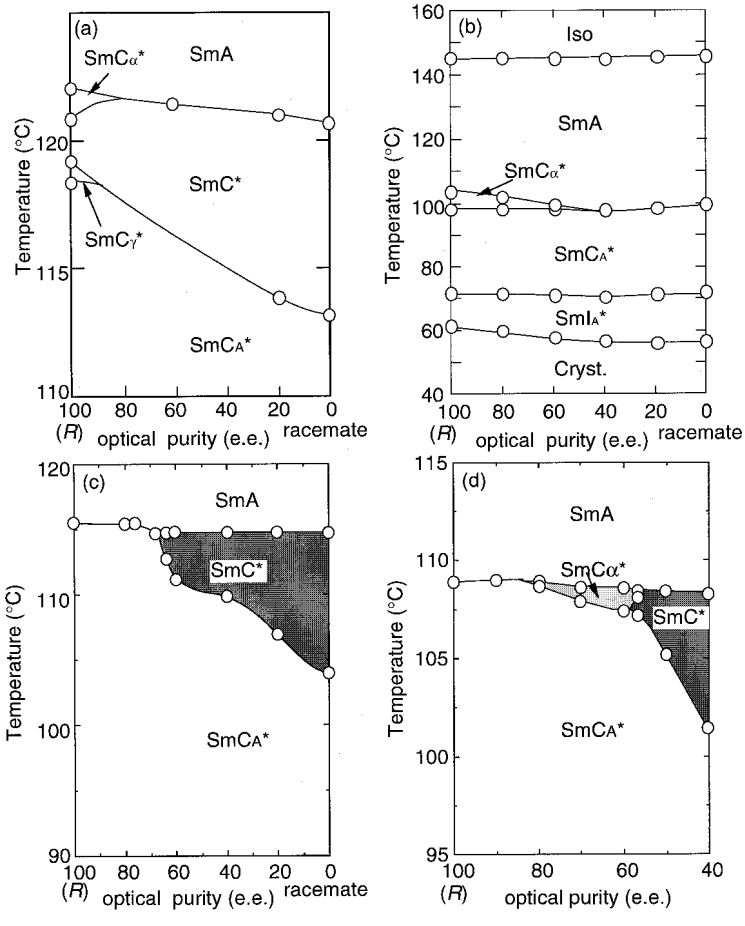

FIGURE 9.22. T–x phase diagrams of isomers with various optical purity in: (a) MHPOBC; (b) MHPOCBC; (c) TFMHPOBC; and (d) TFMHPOCBC.

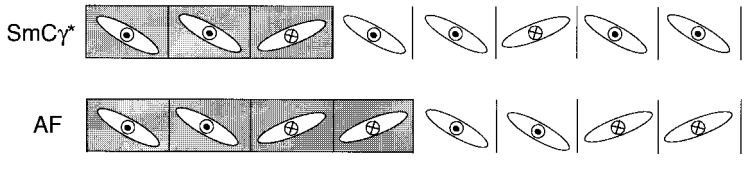

FIGURE 9.23. Molecular orientation structures of the SmCγ^* and AF phases based on the one-dimensional Ising model.

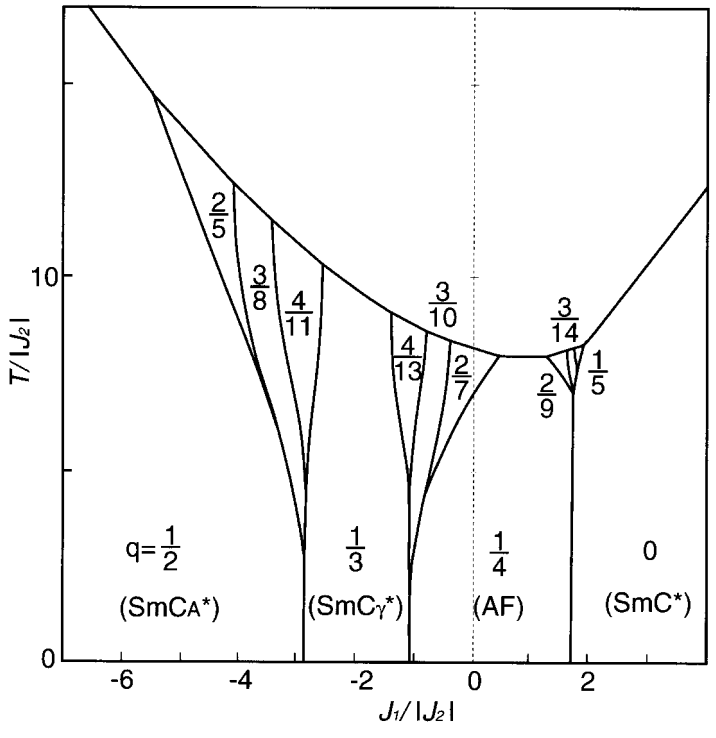

FIGURE 9.24. Phase diagram obtained by the ANNNI model.

Some other subphases were also predicted at finite temperatures. Our treatment and ANNNI + J_3 model give essentially the same structures for the major subphases, SmCγ^* and AF, as displayed in Figure 9.23, although the corresponding rational numbers are different [49].

It is important to note that a macroscopic helix with about a 1 micron pitch is formed even in the Ising model because of the chirality introduced in molecules, so that this tilt plane rotates along the layer normal.

The phenomenological Landau models have been developed by many authors by taking into account the coupling of ferroelectric and antiferroelectric order parameters in bilayer [64]–[68] and axially next-nearest-neighbor (ANNN) interaction [69], [70]. The bilayer models are impractical for SmCγ^*, since no layer spacing change along the layer normal has been observed. The XY character was introduced by considering ANNN interaction (ANNNXY model), leading to a molecular arrangement with very short pitch consisting of three or four layers (spiral model or clock model [69]–[71]; see Figure 9.25). Roy and Madhusudana [70] calculated the phase sequence using the ANNNXY model and succeeded in obtaining the phase sequence SmA–SmCα^*–SmC*–FI_H-FI_I (SmCγ^*)–FI_L–SmC_A^*. Moreover,

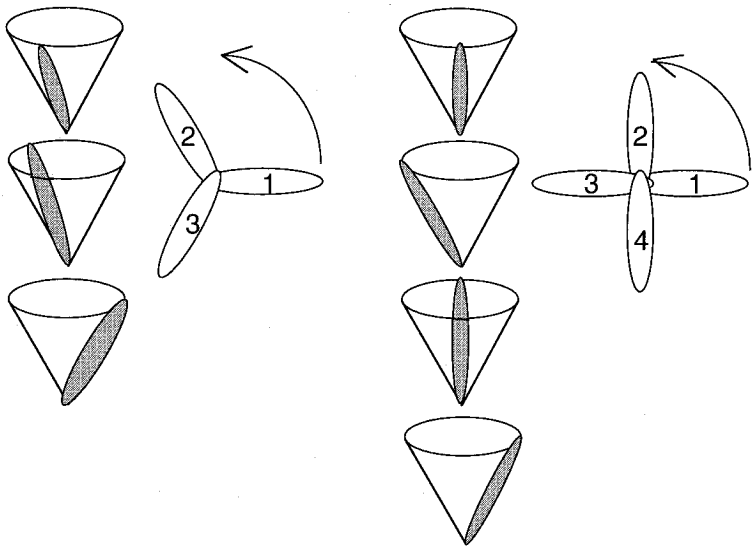

FIGURE 9.25. Molecular arrangements obtained by a spiral or clock model.

they calculated the molecular orientation under the application of an electric field and showed that the clock model, consisting of three layers, is possible to have a metastable state and exhibit a conoscopic figure, which are the same as those observed in SmCγ^* [72]. Recently, Mach et al. [73] performed a resonant X-ray scattering using the free-standing films of sulfur-containing AFLC materials possessing subphases and claimed that the clock model can explain the experimental results.

The XY model gives helical structures with a very short pitch consisting of several layers. Because of such an ultrashort pitch, the system should appear to be optically uniaxial with the optic axis along the layer normal, and to exhibit negligible circular dichroism (CD) and optical rotatory power (ORP). However, macroscopic helices have been observed experimentally not only in $\mathrm{SmC}_{\mathrm{A}}^*$ [74] but also in the subphases. Actually, Miyachi et al. [75], [76] observed laser light diffraction in the SmCγ^* and AF phases of (R)-MHPBC. In this respect, the XY model, particularly the clock model, is not a realistic model for various subphases possessing macroscopic helices. Future studies are necessary to fully understand the appearance of various subphases.

Many attempts to clarify the SmCα^* phase have been made. Experimentally, the following characteristics are known:

(1) It is a tilted phase [77], [78].
(2) Within the phase, various structural changes with temperature and an electric field occur [32], [79], [80].

(3) The helical structure may exist and the pitch length is either very short [78], [81] or very long [82].
(4) A very slow fluctuation mode was observed in dynamic light-scattering measurements [83].
(5) The SmA–SmCα^* phase transition is of the second order and is close to the tricritical point [78], [84].

Future studies are necessary to clarify the structure.

9.5 Frustration Between Ferroelectricity and Antiferroelectricity—V-Shaped Switching

9.5.1 Discovery of V-Shaped Switching and Its Characteristics

As already mentioned, it is well established that many subphases such as antiferroelectric (AF) and ferrielectric (F) phases emerge under the competing interactions for stabilizing ferroelectricity and antiferroelectricity. This situation can be described as a competition between synclinic and anticlinic interactions, namely, the interlayer tilting correlation. A decrease in the degree of the tilting correlation or the frustration of ferroelectricity and antiferroelectricity brings about another interesting phenomenon; i.e., V-shaped switching characterized by thresholdless, hysteresis-free, and domainless behavior.

For the V-shaped switching, Inui et al. [85] and Fukuda et al. [86] have suggested a phase with randomly oriented C-directors due to the reduction of the interlayer tilting correlation, without any piece of experimental evidence. The dynamic switching behaviors seemed to be explained by the random model based on the two-dimensional Langevin function [85]. However, the phase with randomly oriented C-directors has never yet been confirmed.

So far, only two mixtures composed of two and three compounds (Figure 9.26) showing V-shaped switching have been reported [85]–[94]. These mixtures show ambiguous phase sequences such as the ferrielectric phases over a wide temperature range in the bulk states [89], [90]. Since the ferrielectric phases are known to appear due to the competition (frustration) between interactions stabilizing ferroelectricity and antiferroelectricity, it is reasonable to consider that the phase, in which the interlayer correlation or the tilting correlation is reduced, manifests itself by V-shaped switching.

Thin homogeneously aligned cells showing V-shaped switching exhibit a uniformly dark view in the absence of a field under crossed polarizers, one of which is parallel to a smectic layer. If there are ferroelectric and/or ferrielectric domains, the size of which is larger than the wavelength of the visible light, one can see domains with different brightness.

The evolution of switching characteristics from tristable to V-shaped was

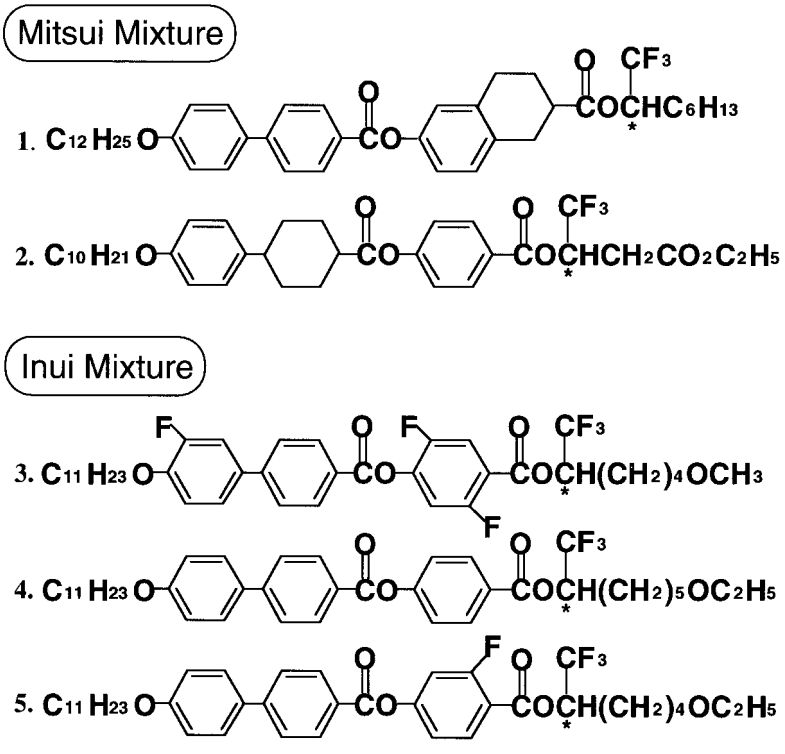

FIGURE 9.26. Materials showing V-shaped switching, two mixtures/five compounds.

observed with increasing temperature and frequency in an apparently AFLC (compound 3 in Figure 9.26), as shown in Figure 9.27 [89]. In the electro-optic response at 23 °C and at 0.1 Hz, the evolution is clearly seen because of the accidental difference of the two substrate surface conditions: The stable state is the antiferroelectric phase. However, it is clear that the dark state at 0 V dynamically driven (arrow 1) has a different structure from the ordinary antiferroelectric structure (arrow 2) which also shows a dark view, since there is no reason that the same arrangement emerges twice in a quarter-period of switching. Then, the questions are as follows:

(1) What is the stable molecular orientation at 0 V;
(2) What is the dynamics of the switching? and
(3) What is the origin of the particular stable orientation at 0 V?

9.5.2 *Collective Motion During V-Shaped Switching*

Park et al. [92] measured the effective optical anisotropy Δn_{eff}, the apparent tilt angle θ_{app}, the switching current, and the second-harmonic generation in the three-component mixture (3:4:5 = 40:40:20 (wt%) in Figure 9.26) and

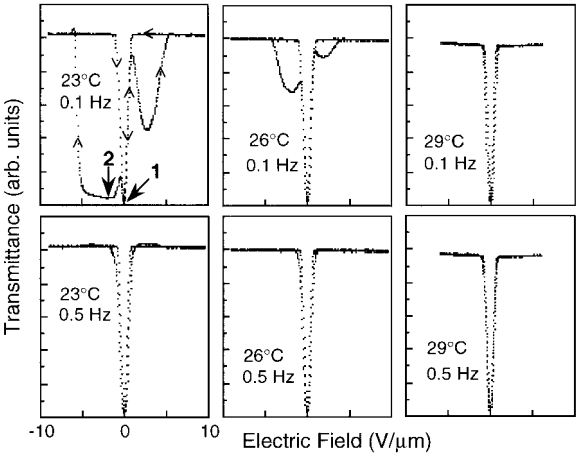

FIGURE 9.27. Transmittance versus electric field on applying a triangular waveform of 0.1 Hz and 0.5 Hz at 23 °C, 26 °C, and 29 °C in a homogeneously aligned cell of the compound 3 of Figure 9.26. Note that evolution is observed from tristable to V-shaped switching by changing the frequency and temperature.

compared them with the simulated results based on two extreme models, i.e., the random model and the collective model, where molecules switch randomly and collectively, respectively. The comparison revealed that the collective switching motion of liquid crystal molecules is more reasonable than the random motion, as will be shown in the following. Moreover, it was also confirmed that the observed infrared absorption anisotropy of the phenyl stretching mode due to liquid crystal molecular distributions strongly supports the collective model.

Figure 9.28 illustrates the electro-optic responses observed at two Θ's; 0° and 30°, where Θ is the angle between the layer normal and one of the crossed polarizer directions. As shown in Figure 9.28 [92], the electric field dependence of transmittance at $\Theta = 0°$ shows the typical thresholdless, hysteresis free, V-shaped switching. From the electro-optic measurements at every 5° of Θ, the transmittance T versus Θ was obtained at given electric fields. Figure 9.29(a) shows three examples of T versus Θ curves at applied fields of 0, +6, and −6 V/μm [92]. The transmittance T is described by

$$T = \sin^2(2(\Theta + \theta_{\text{app}}))\sin^2\left(\frac{\pi \Delta n_{\text{eff}} d}{\lambda}\right), \tag{9.2}$$

where d is the cell thickness and λ the light wavelength. Normally, the electro-optic transmittance change at fixed temperatures is regarded as a function of only $\theta_{\text{app}}(F)$, where F is an applied electric field. However, θ_{app} is also a function of F, since θ_{app} is determined by molecular distribution. Park et al. [92] analyzed Δn_{eff} as well as θ_{app} as a function of F. As is easily seen in

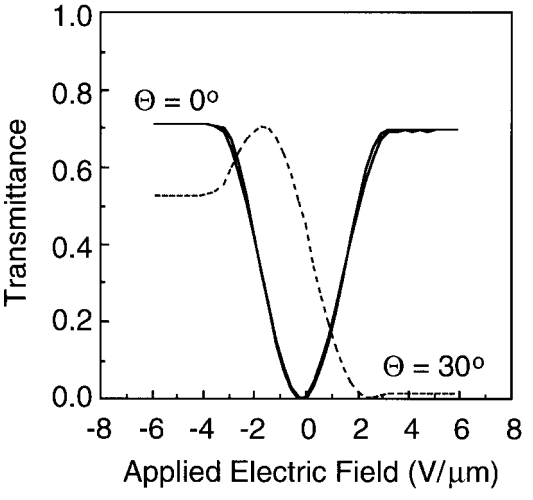

FIGURE 9.28. The electro-optic responses observed in a homogeneous cell during the application of a triangular wave of 0.1 Hz for $\Theta = 0°$ and 30°.

(9.2), the amplitude and the phase of the T–Θ curve give Δn_{eff} and θ_{app} at a given electric field, respectively. Figures 9.29(b) and (c) show θ_{app} and Δn_{eff} of the V-shaped switching cell as a function of the applied electric field, respectively.

Simulation of θ_{app} and Δn_{eff} was made for the two extreme models, i.e., the random and collective models. The results are shown by solid (collective) and broken (random) curves in Figure 9.29(c). It is clear that the calculated Δn_{eff} for the collective model with a layer tilt angle of 8° is the same as the experimental result, while the random model gives serious disagreement. From these results, it is clear that the collective behavior of liquid crystal molecules is more reasonable than the random distribution for the V-shaped switching.

Very intuitive evidence of the molecular uniform orientation in the absence of a field is given by polarized IR absorption [92]. Figure 9.30(a) shows the polar plot of the polarized IR absorbance of phenyl ring stretching observed as a function of a polarizer rotation angle in the SmA phase [92]. Large anisotropy between 0° (layer direction) and 90° (layer normal direction) is observed. In the SmX phase exhibiting V-shaped switching at zero electric field, an absorption maximum of the phenyl ring stretching appears in the same direction as in SmA, as shown in Figure 9.30(b). Moreover, it is noted that the anisotropies of both phases are almost the same. This observation suggests that the molecular orientational order in the SmX phase at zero field is almost the same as that in the SmA phase. By applying high dc electric fields in SmX to obtain the SmC* orientation, the absorption maximum direction rotates by a tilt angle of about 35°, as shown in Figure 9.30(c). If random distribution is achieved, the anisotropy must be much smaller than that in Figure 9.30(b). Actually, the absorption in the AF phase

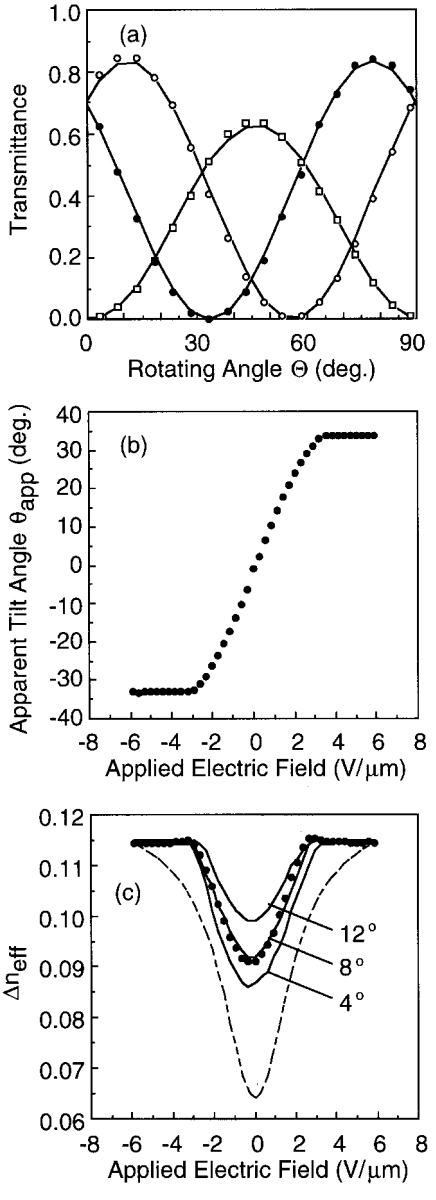

FIGURE 9.29. (a) The rotating angle dependences of transmittance (T–Θ for $F = +6$ V/μm (closed circles), 0 V/μm (open squares), and -6 V/μm (open circles). (b) The apparent tilt angle θ_{app} as a function of applied electric field. (c) Δn_{eff} as a function of the applied electric field. Solid and broken lines are simulated results using the collective and random models, respectively. The collective model with a layer tilt of 8° fits perfectly [92].

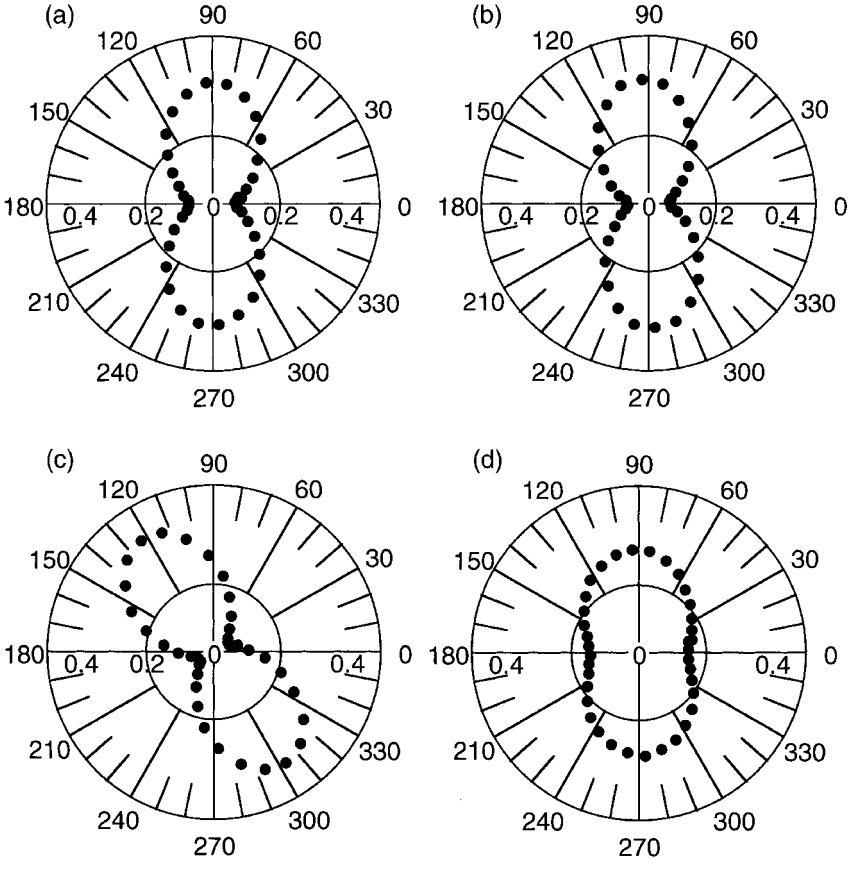

FIGURE 9.30. Polar plots of the absorbances of the phenyl ring (1605 cm^{-1}) stretching mode versus the polarizer rotation angle in a homogeneously aligned liquid crystal cell: (a) SmA; (b) SmX* without applied field; (c) SmX* with $F = +5$ V/μm; and (d) antiferroelectric without applied field [92].

(20 °C) using the same cell shows small anisotropy at zero field, as shown in Figure 9.30(d), because of the antiferroelectric molecular ordering. These results clearly show that the SmX* phase exhibiting V-shaped switching definitely has a different molecular orientation from that in the antiferroelectric phase and the random orientation but has rather uniform orientation.

Second-harmonic generation (SHG) also gives useful information. Strong optical SHG signals have been observed unexpectedly at normal incidence from the V-shaped switching liquid crystal cell [92], [93]. This result seemed to be also explained by the two-dimensional Langevin potential, supporting the random model [93]. However, the collective model is much more appropriate to interpret the V-shaped switching than the random model, as will be shown in the following.

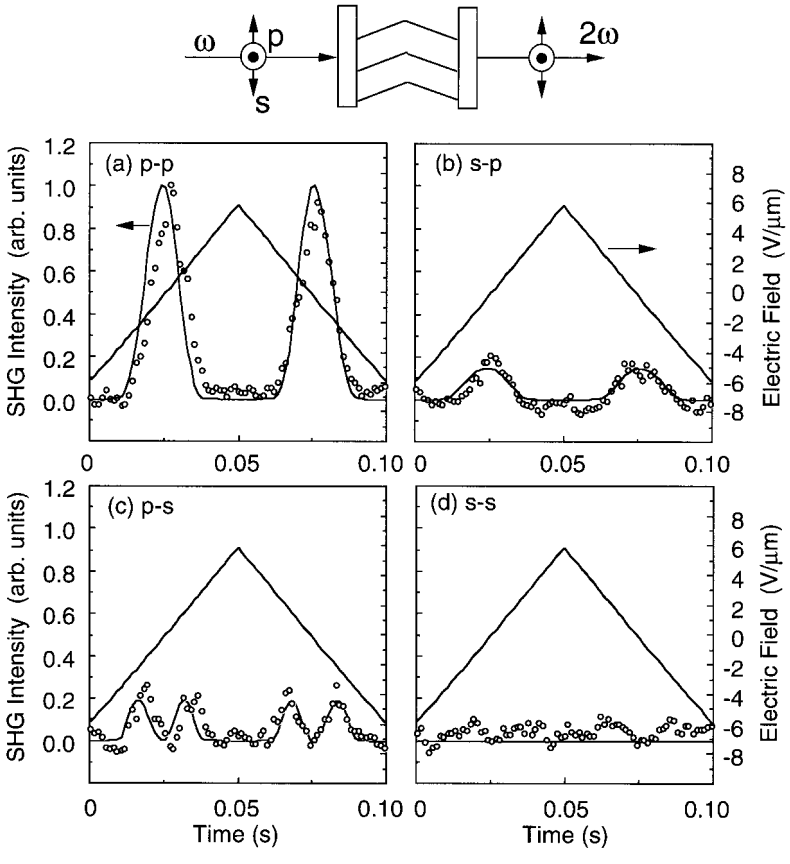

FIGURE 9.31. Second-harmonic generation intensity profiles as a function of the applied electric field for four input/output polarization combinations, i.e., *p–p* (*p*-in/*p*-out), *s–p*, *p–s*, and *s–s* at normal incidence in the optical geometry shown at the top of the figure [94].

Figure 9.31 shows the SHG intensity profiles as a function of an applied electric field for four input/output polarization combinations, i.e., *p–p* (*p*-in/*p*-out), *s–p*, *p–s*, and *s–s* at normal incidence [94], where *p*- and *s*-polarizations are defined as polarizations parallel and perpendicualr to the smectic layer. These SHG behaviors are characteristics of the V-shaped switching because the SHG cannot be observed in normal ferroelectric bistable switching, in which the dipole direction in the field-induced ferroelectric uniform state is perpendicular to the electric field direction of incident light and switches instantaneously to the opposite direction. Solid curves in Figure 9.31 show the best fitted SHG intensity profiles simulated using the collective model. As shown in the figure, it is clear that the calculated SHG profiles are identically the same as the experimental results.

9.5.3 *Mechanism of V-Shaped Switching*

One of the major advantages of using SHG measurement can be attributed to SHG interferometry, which gives the information of the phase of the signal or the orientational sense of the polar order. For the SHG interference measurement, a crystal quartz plate was inserted in the optical path [95]. Then, second-harmonic waves were generated both from the quartz plate and the sample and interfered with each other. A fused silica plate was located between the quartz plate and the sample cell, and was rotated about the axis parallel to the fused silica plate and perpendicular to the optical path, producing a relative phase change between second-harmonic waves from the two sources because of a frequency dispersion of the refractive index of the fused silica plate. In this way, one can observe interference fringes.

Figure 9.32 shows interferograms of SHG peaks obtained by rotating the fused silica plate for positive and negative slopes of applied fields during the switching [94]. As shown in Figure 9.32(a), it is obvious that the phase of the SHG fringe is not reversed in the opposite slopes of an applied electric field for *p–p* geometry. This fact indicates that the (nonlinear) polarization at about zero field has the same orientational sense in both the positive and negative slopes of a field. Namely the polarization switches on one-half of the smectic cone back and forth. Note that, for *p–s*, the phase of interferogram for inner SHG peaks (Figure 9.32(b)) is out of phase to that for outer SHG peaks (Figure 9.32(c)).

Now the question is why and how molecules choose one-half of the cone for the switching. If the smectic layer is of bookshelf type, there is no reason to choose either half of the cone. However, there exists a chevron structure, as was confirmed using a separate cell by X-ray analysis. Then molecules can choose one-half (actually less than 180°) of the azimuthal angle on the cone, since molecules have a tendency to align themselves parallel to a substrate surface, as illustrated in Figure 9.33 ($E = 0$). If the volume of the upper and lower halves of the chevron structure is not the same, SHG would be observed. This situation is illustrated in Figure 9.33: The liquid crystal molecules rotate toward the opposite directions in the upper and lower halves of the chevron structure.

In this way, collective molecular switching occurs, as illustrated in Figure 9.33. It is clear that the directional senses of the *p*-polarized second-harmonic light in positive and negative slopes of the field are the same, as experimentally observed. On the other hand, it is also easy to understand that two peaks appear for the *s*-polarized SHG at positive and negative sides of the zero field and have the opposite phases, and that the outer (inner) peaks in positive and negative slopes have the same phase, as also observed experimentally. Thus, the simple collective model shown in Figure 9.33 satisfies all the experimental results of SHG intensity and SHG interferometry.

The next problem is the cause and the mechanism of the V-shaped

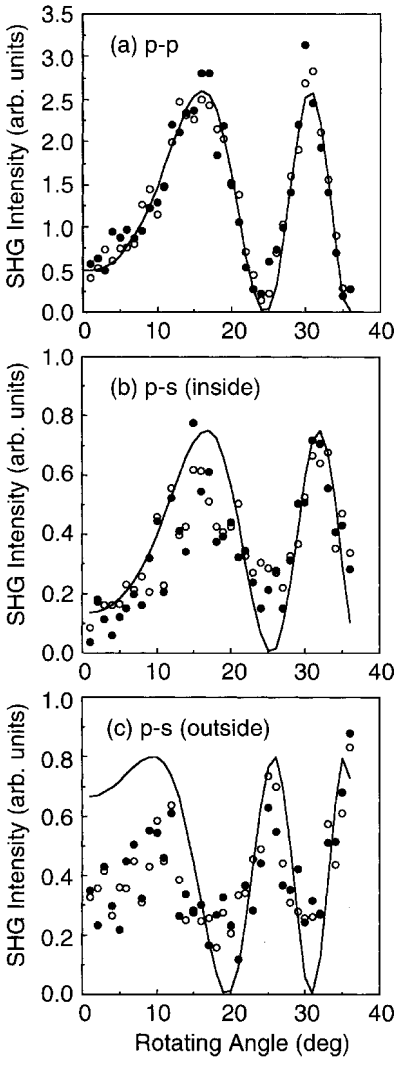

FIGURE 9.32. Interference fringes of (a) SHG peak for *p–p*, (b) inner peak for *p–s*, and (c) outer peak for *p–s* observed by rotating a fused silica plate during positive (open circles) and negative (closed circles) slopes of an applied electric field. Solid curves show the calculated interference fringes [94].

switching. The first important question is why the molecules take the uniform orientation shown in Figure 9.33 at zero field. We would like to point out the effect of polarization space charge ρ given by $-\mathrm{div}\, P$, where P is a polarization [96], [97]. It is well known that polar surface interaction stabilizes a twisted state [98], in which a splay deformation of P exists. Then the polarization space charge is produced. This effect is pronounced when P becomes large. Hence molecules tend to form a uniform orientation shown in Figure 9.33 ($E = 0$) to avoid the production of the polarization charge.

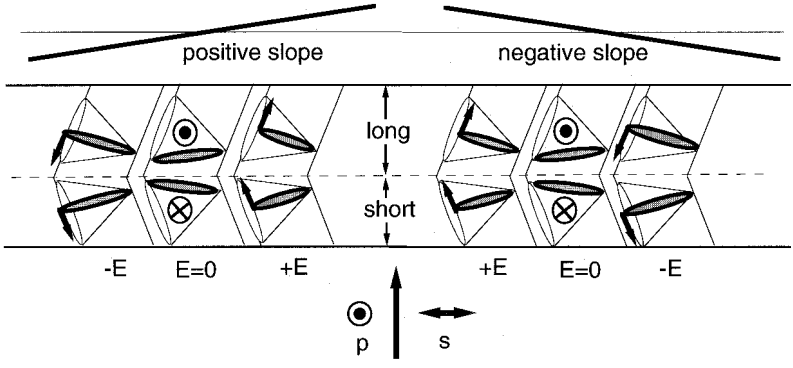

FIGURE 9.33. Illustration of the collective switching model for the V-shaped switching.

The twisted structure only at the surface area of less than 0.1 μm thick is allowed to give almost completely dark.

The next question is why molecules switch collectively. The V-shaped switching occurs in the system where ferroelectric and antiferroelectric interactions compete and frustration between these structures takes place [99], [100]. Since such a frustrated system is very soft and the relaxation time becomes long, molecules change their steady-state orientation continuously under the surface constraint and varying field, resulting in the collective motion.

Questions still exist; the SmX* phase exhibiting V-shaped switching is a new phase or there are some conventional phases such as ferroelectric, antiferroelectric, and ferrielectric phases. One of the most important experiments remaining is the quantitative measurement of the tilting correlation between adjacent layers. This is a future problem.

9.6 Electro-optic Applications

9.6.1 Tristable Switching

So far, four display modes have been proposed in ferroelectric and antiferroelectric display applications, as shown in Figure 9.34. A bistable switching in surface stabilized ferroelectric liquid crystals (SSFLCs) has been manufactured as a passive matrix liquid crystal display (PM-LCD). The counterpart of AFLC is a tristable switching, which is also a promising candidate for PM-LCD. In addition to these PM-LCDs, active matrix displays (AM-LCDs) are also proposed in FLC and AFLC materials, i.e., deformed helix FLCD (DHFLC) and V-shaped LCD (VLCD). In this section, PM-AFLCD and AM-VLCD will be described.

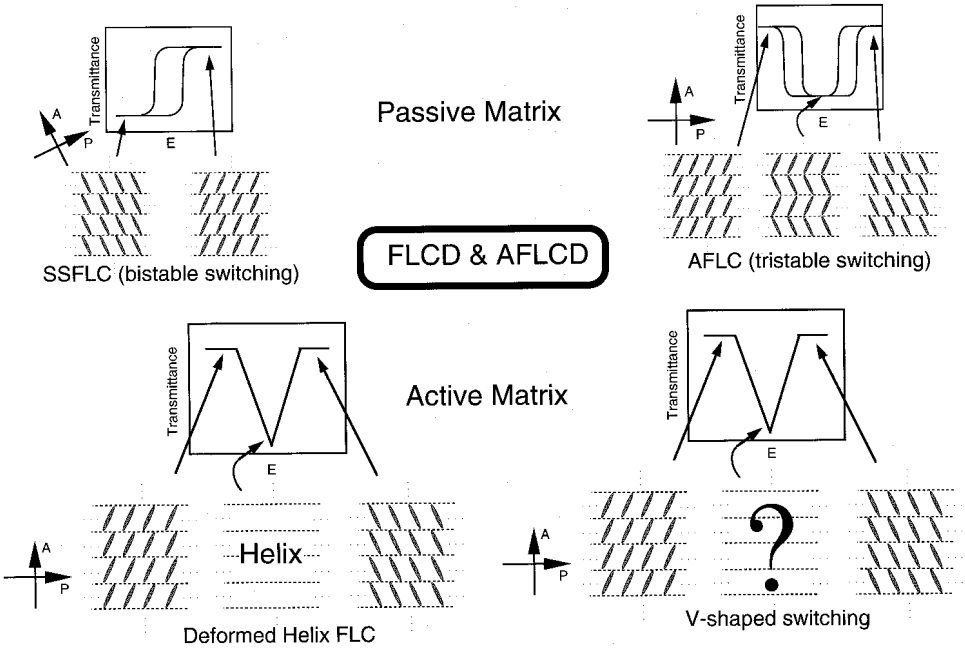

FIGURE 9.34. Four display modes proposed in ferroelectric and antiferroelectric display applications.

Tristable switching is based on the field-induced antiferroelectric–ferroelectric (AF–F) phase transition, as already mentioned in Section 9.1. A well-aligned cell is placed between crossed polarizers, one of which is parallel to the smectic layer. Then a dark view is obtained in the absence of a field. By applying a field, the AF–F phase transition takes place and the view turns bright due to optical birefringence. Because of this switching mode, the viewing angle is very wide.

The fundamental concept of the driving scheme for PM-AFLCD [11] is shown in Figure 9.35. The driving is made by applying a pulsed voltage (V_D or V_N) in addition to a bias voltage (V_0) which is between high and low threshold voltages (V_{th}^H and V_{th}^L, respectively) forming a hysteresis. For $V_D + V_0 > V_{th}^H$, switching occurs, while for $V_N + V_0 < V_{th}^H$, switching does not occur. In the multiplexing, hystereses on the positive and negative sides were used alternatively. Because of this scheme, charge accumulation which causes the so-called ghost effect is not so serious.

The response speed depends on the effective voltage that is the difference between the applied voltage and the threshold voltage (Figure 9.35). Figure 9.36 shows the transmittance changes (a) from AF to F and (b) from F to AF in MHPOBC [101]. In both cases, the lower voltage of a rectangular field

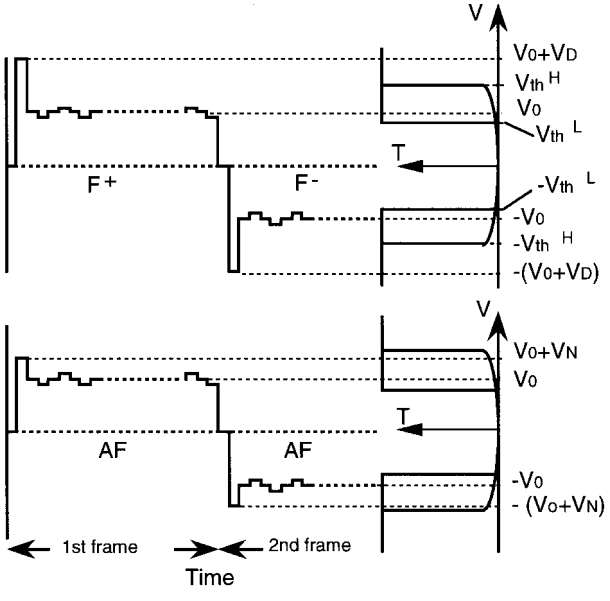

FIGURE 9.35. Fundamental concept of driving scheme for PM-AFLCD.

was fixed at 0 V in the AF state and the voltage in the F state was varied from 32 V to 38 V. As shown in Figure 9.36(a), 28 V is too low to induce the AF–F phase transition (below the threshold voltage V_{th}^{H}). Whilst the response time markedly depends on the higher voltage applied for the AF–F switching, it is independent of the higher voltage for the F–AF switching. Another noticeable feature is the two-step change for the AF–F switching. At the first step, a very fast switching to a certain transmittance occurs and then slowly (particularly at low voltages) changes to the maximum transmittance in the F state. The first metastable transmittance level corresponds to the transmittance in the AF state at the threshold voltage and is attributed to a pretransitional effect for the AF–F transition. This phenomenon can be ascribed so that the anticlinic molecular arrangement in adjacent layers is slightly deformed owing to a change in the azimuthal angle. As a result, it leads to the leakage of the transmittance in the AF state and brings about a serious problem for display application, i.e., low contrast ratio. Therefore, the materials which exhibit negligible pretransitional effect are required for application.

The response time for the AF–F and F–AF switching is shown in Figure 9.37 for the stepwise voltage change (a) from 0 V and the stepwise voltage drop (b) from 30 V [101]. Figure 9.37 clearly indicates that the response time remarkably depends on the effective voltage. The response time as a function

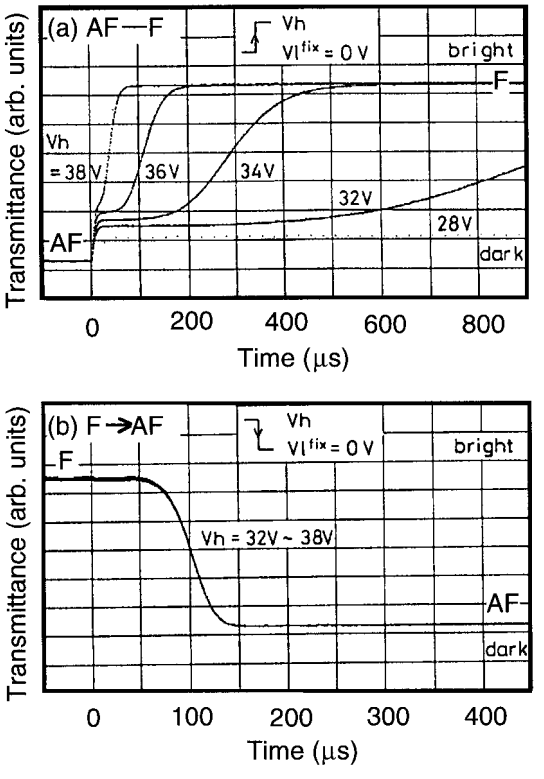

FIGURE 9.36. The transmittance changes (a) from AF to F and (b) from F to AF in MHPOBC [101].

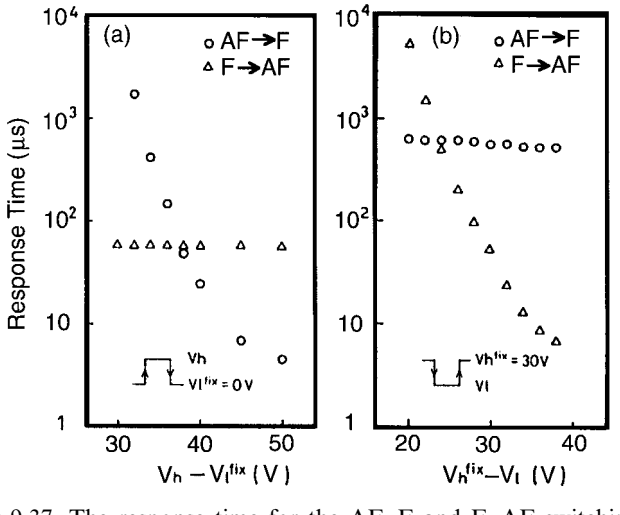

FIGURE 9.37. The response time for the AF–F and F–AF switching in MHPOBC [101].

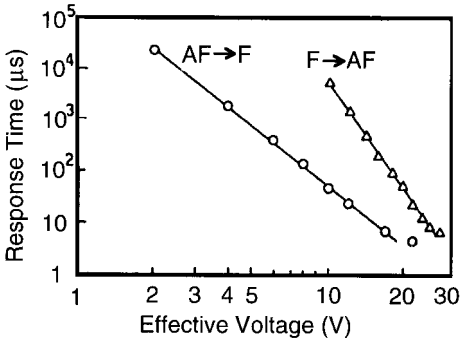

FIGURE 9.38. The response time as a function of effective voltage in MHPOBC [101].

FIGURE 9.39. 17 inch AFLC display developed by DENSO CORP.

of the effective voltage is shown in Figure 9.38. The dependence of the fourth power and seventh power was obtained for the AF–F and F–AF switching, respectively. The response time is very fast, if we apply high effective voltages. The applied voltage, which is equal to a sum of the effective voltage and the threshold voltage, is necessarily high. This is one of the disadvantages for the tristable AFLC display.

A gray level can be achieved by utilizing domain formation associated with the field-induced AF–F phase transition. At the transition, ferroelectric striped domains are nucleated at the electrode edges and grow along smectic layers [101], [102]. Therefore, the area could be controled by the height or duration of the pulses applied. Actually, full color displays have been developed by several companies. Figure 9.39 shows a photograph of 17 inch AFLCs display developed by DENSO.

9.6.2 V-Shaped Switching

The V-shaped switching mode mentioned in the previous section provides us with another promising display mode. The switching is associated with nei-

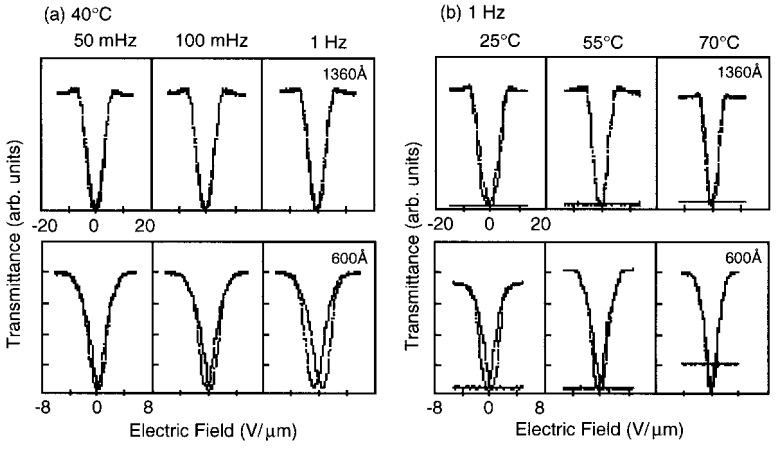

FIGURE 9.40. (a) The optical transmittance measured at 40 °C by applying triangular voltage waves of 50, 100, and 1000 mHz for the cells coated with polyimide films of two different thicknesses. (b) The V-shaped switching measured at a frequency of 1 Hz and at 25 °C, 55 °C, and 70 °C for polyimide films of two different thicknesses [103].

ther threshold nor hysteresis. The switching is not associated with domain formation. The cell always gives a dark appearance, whenever an applied field is turned off.

The performance is sometimes influenced by surface conditions. Chandani et al. [91] systematically studied the effect of the surface alignment layer using a liquid crystal compound 5 in Figure 9.26, and concluded that thick alignment layers and less polar surfaces are ideal for V-shaped switching. Figure 9.40(a) compares the optical transmittance measured at 40 °C by applying triangular voltage waves of 50, 100, and 1000 mHz for the cells coated with a polyimide for DHFLC of two different thicknesses [103]. At these frequencies, V-shaped and W-shaped switchings were favorable for 1360 Å and 600 Å films, respectively. The bottom line (abscissa) corresponds to the complete dark state when no light goes to the photomultiplier tube. A comparison of the V-shaped switching measured at a frequency of 1 Hz with varied temperatures at 25 °C, 55 °C, and 70 °C for two different PI-DHFLC film thicknesses is shown in Figure 9.40(b). The solid straight line in each figure shows the transmittance when the field is switched off. For both thicknesses, the transmittance remains at low level when the field is switched off, unless the temperature is high (70 °C) and the PI-DHFLC film is thin (600 Å). Thus a thicker alignment layer assists in achieving V-shaped switching [103].

However, when the alignment layer becomes thicker, a higher driving field is necessary; this may be a disadvantage from an application point of view. Instead of using a thick polyimide film, the capacitance was decreased by using a thin polyimide film (600 Å) together with an insulating layer, i.e.,

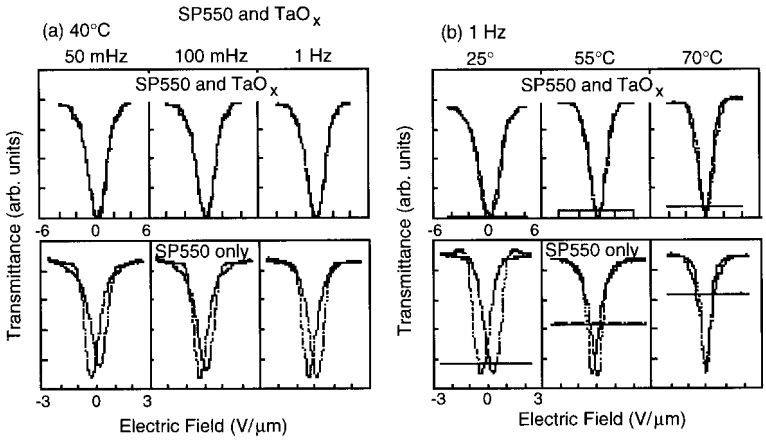

FIGURE 9.41. (a) The optical transmittance measured at 40 °C and at different frequencies for polyimide SP550 (600 Å) with and without the insulating layer. (b) The temperature-dependence of the optical response measured at 1 Hz frequency for the cells with and without the insulating layer [103].

TaO_X of 900 Å thickness. Figure 9.41(a) compares the optical transmittance measured at 40 °C and at different frequencies for a polyimide film (Toray, SP550, 600 Å) with and without the insulating layer. As the SP550 film is relatively thinner (600 Å) it gives rise to W-shaped switching without an insulating layer. When TaO_X was used as the insulating layer with a thin SP550, good V-shaped switching was observed. Figure 9.41(b) illustrates the temperature-dependence of the optical response measured at 1 Hz frequency for the cells with and without the insulating layer. The transmittance in the field-off state became very low when the insulating layer was used. From this figure it is clear that good V-shaped switching can be achieved when TaO_X is used as an insulating layer together with thin PI-DHFLC and SP550 at all temperatures and frequencies. Thus, less polar TaO_X, which has a high dielectric constant, favors V-shaped switching. In this way, to achieve an ideal V-shaped switching, an appropriate choice of a surface alingment layer and an insulating layer in addition to smectic liquid crystal materials is very important.

Because of no threshold behavior, the mode can be utilized as AM-LCD in conjunction with TFT. The continuous change in the transmittance is suitable for full color display. Since a very dark view is realized in the absence of a field, a high contrast ratio more than 100 could be easily achieved. At present at least Toshiba and Casio announced their prototype LCD using V-shaped switching, as shown in Figure 9.42. Specifications of these displays in addition to DENSO PM-AFLCD are shown in Figure 9.43. These photographs clearly reveal a good viewing angle. Because of its high display performance such as a wide viewing angle, high contrast, full color, and high

FIGURE 9.42. AM-VLCD developed by Toshiba and Casio.

	DENSO	TOSHIBA	CASIO
type	PM (tristable)	AM (V-shape)	AM (V-shape)
size	17.4 inch	15 inch	5.5 inch
resolution	1280 x 1024	1024 x 768	240 x 320
contrast	50 : 1	>100 : 1	300 : 1
viewing angle	160°	140°	160°
gray scale	16.7 M color	0.262 M color	16.7 M color
driving voltage	higer than normal TFT	±5 V	±2.5 V
temp. range	0°C~35°C	——	-30°C~60°C

FIGURE 9.43. Specifications of the display by DENSO CORP., Toshiba and Casio.

speed, the V-shaped switching display is considered as a candidate for next-generation display.

References

[1] R.B. Meyer, L. Liebert, L. Strzelecki, and P. Keller, *J. Phys. (France)* **36**, L69 (1975).

[2] T. Inukai, K. Furukawa, K. Terashima, S. Saito, M. Isogai, T. Kitamura, and A. Mukoh, *Abstract Book of Japan Domestic Liq. Cryst. Meeting*, Kanazawa, p. 172 (in Japanese), 1985.

[3] N. Hiji, A.D.L. Chandani, S. Nishiyama, Y. Ouchi, H. Takezoe, and A. Fukuda, *Ferroelectrics* **85**, 99 (1988).

[4] K. Furukawa, K. Terashima, M. Ichihashi, S. Saitoh, K. Miyazawa, and T. Inukai, *Ferroelectrics* **85**, 63 (1988).

[5] A.M. Levelut, C. Germain, P. Keller, and L. Liebert, *J. Phys. (France)* **44**, 623 (1983).

[6] Y. Galerne and L. Liebert, *Abstract Book of 2nd International Conf. Ferroelectric Liq. Cryst.* **O27** (1989).

[7] H. Takezoe, A.D.L. Chandani, J. Lee, E. Gorecka, Y. Ouchi, A. Fukuda, K. Terashima, K. Furukawa, and A. Kishi, *Abstract Book of 2nd International Conf. Ferroelectric Liq. Cryst.* **O26** (1989).

[8] H. Takezoe, A.D.L. Chandani, E. Gorecka, Y. Ouchi, and A. Fukuda, *Abstract Book of 2nd International Conf. Ferroelectric Liq. Cryst.* **P108** (1989).

[9] J.W. Goodby and E. Chin, *Liq. Cryst.* **3**, 1245 (1988).

[10] A.D.L. Chandani, T. Hagiwara, Y. Suzuki, Y. Ouchi, H. Takezoe, and A. Fukuda, *Jpn. J. Appl. Phys.* **27**, L729 (1988).

[11] N. Yamamoto, Y. Yamada, N. Koshobu, K. Mori, K. Nakamura, H. Orihara, Y. Ishibashi, Y. Suzuki, and I. Kawamura, *Jpn. J. Appl. Phys.* **31**, 3182 (1992).
[12] A.D.L. Chandani, E. Gorecka, Y. Ouchi, H. Takezoe, and A. Fukuda, *Jpn. J. Appl. Phys.* **28**, L1265 (1989).
[13] Y. Galerne and L. Liebert, *Phys. Rev. Lett*. **64**, 906 (1990).
[14] Y. Takanishi, H. Takezoe, M. Johno, T. Yui, and A. Fukuda, *Jpn. J. Appl. Phys.* **32**, 4605 (1993).
[15] P. Cladis and H.R. Brand, *Liq. Cryst.* **14**, 1327 (1993).
[16] G. Heppke, P. Kleineberg, D. Lötzsch, S. Mery, and R. Shashidhar, *Mol. Cryst. Liq. Cryst*. **231**, 257 (1993).
[17] Ch. Bahr and D. Fliegner, *Phys. Rev. Lett.* **70**, 1842 (1993).
[18] Y. Takanishi, H. Takezoe, A. Fukuda, H. Komura, and J. Watanabe, *J. Mater. Chem.* **2**, 71 (1992)
[19] Y. Takanishi, H. Takezoe, A. Fukuda, and J. Watanabe, *Phys. Rev. B* **45**, 7684 (1992).
[20] E. Gorecka, A.D.L. Chandani, Y. Ouchi, H. Takezoe, and A. Fukuda, *Jpn. J. Appl. Phys.* **29**, 131 (1990).
[21] T. Fujikawa, K. Hiraoka, T. Isozaki, K. Kajikawa, H. Takezoe, and A. Fukuda, *Jpn. J. Appl. Phys.* **32**, 985 (1993).
[22] K. Hiraoka, A. Taguchi, Y. Ouchi, H. Takezoe, and A. Fukuda, *Jpn. J. Appl. Phys.* **29**, L103 (1990).
[23] K. Hiraoka, Y. Ouchi, H. Takezoe, and A. Fukuda, *Mol. Cryst. Liq. Cryst.* **199**, 197 (1991).
[24] K. Itoh, Y. Takanishi, J. Yokoyama, K. Ishikawa, H. Takezoe, and A. Fukuda, *Jpn. J. Appl. Phys.* **36**, L784 (1997).
[25] Y. Suzuki, T. Hagiwara, I. Kawamura, N. Okamura, T. Kitazume, M. Kakimoto, Y. Imai, Y. Ouchi, H. Takezoe, and A. Fukuda, *Liq. Cryst.* **6**, 167 (1989).
[26] H. Takezoe, J. Lee, A.D.L. Chandani, E. Gorecka, Y. Ouchi, and A. Fukuda, *Ferroelectrics* **114**, 187 (1991).
[27] T. Isozaki, H. Takezoe, A. Fukuda, Y. Suzuki, and I. Kawamura, *J. Mater. Chem.* **4**, 237 (1994).
[28] H. Takezoe, A. Fukuda, A. Ikeda, Y. Takanishi, T. Umemoto, J. Watanabe, H. Iwane, M. Hara, and K. Itoh, *Ferroelectrics* **122**, 167 (1991).
[29] A. Ikeda, Y. Takanishi, H. Takezoe, A. Fukuda, S. Inui, S. Kawano, M. Saito, and H. Iwane, *Jpn. J. Appl. Phys.* **30**, L1032 (1991).
[30] S. Inui, S. Kawano, M. Saito, H. Iwane, Y. Takanishi, K. Hiraoka, Y. Ouchi, H. Takezoe, and A. Fukuda, *Jpn. J. Appl. Phys.* **30**, L1032 (1990).
[31] A. Ikeda, Y. Takanishi, H. Takezoe, and A. Fukuda, *Jpn. J. Appl. Phys.* **32**, L97 (1993).
[32] Y. Takanishi, K. Hiraoka, V.K. Agrawal, H. Takezoe, A. Fukuda, and M. Matsushita, *Jpn. J. Appl. Phys.* **30**, 2023 (1991).
[33] K. Miyachi, J. Matsushima, Y. Takanishi, K. Ishikawa, H. Takezoe, and A. Fukuda, *Phys. Rev. E* **52**, R2158 (1995).
[34] I. Nishiyama and J.W. Goodby, *J. Mater. Chem.* **3**, 149 (1993).
[35] T. Kusumoto, T. Isozaki, Y. Suzuki, Y. Takanishi, H. Takezoe, A. Fukuda, and T. Hiyama, *Jpn. J. Appl. Phys.* **34**, L830 (1995).
[36] Y. Suzuki, T. Isozaki, S. Hashimoto, T. Kusumoto, T. Hiyama, Y. Takanishi, H. Takezoe, and A. Fukuda, *J. Mater. Chem.* **6**, 753 (1996).

[37] J. Watanabe and M. Hayashi, *Macromolecules* **22**, 4083 (1989).
[38] K. Hori and K. Endo, *Bull. Chem. Soc. Jpn.* **66**, 46 (1993).
[39] K. Hori, S. Kawahara, and K. Ito, *Ferroelectrics* **147**, 91 (1993).
[40] S. Yoshida, B. Jin, Y. Takanishi, K. Tokumaru, K. Ishikawa, H. Takezoe, A. Fukuda, T. Kusumoto, T. Nakai, and S. Miyajima, *J. Phys. Soc. Jpn.* **68**, 9 (1999).
[41] T. Nakai, S. Miyajima, Y. Takanishi, S. Yoshida, and A. Fukuda, *J. Phys. Chem. B* **103**, 406 (1999).
[42] B. Jin, Z. Ling, Y. Takanishi, K. Ishikawa, H. Takezoe, A. Fukuda, M. Kakimoto, and T. Kitazume, *Phys. Rev. E* **53**, R4295 (1996).
[43] Y. Ouchi, Y. Yoshioka, H. Ishii, K. Seki, M. Kitamura, R. Noyori, Y. Takanishi, and I. Nishiyama, *J. Mater. Chem.* **5**, 2297 (1995).
[44] N. Okabe, Y. Suzuki, I. Kawamura, T. Isozaki, H. Takezoe, and A. Fukuda, *Jpn. J. Appl. Phys.* **31**, L793 (1992).
[45] A.D.L. Chandani, Y. Ouchi, H. Takezoe, A. Fukuda, K. Terashima, K. Furukawa, and A. Kishi, *Jpn. J. Appl. Phys.* **28**, L1261 (1989).
[46] M. Fukui, H. Orihara, Y. Yamada, N. Yamamoto, and Y. Ishibashi, *Jpn. J. Appl. Phys.* **28**, L849 (1989).
[47] K. Ema, H. Yao, I. Kawamura, T. Chan, and C.W. Garland, *Phys. Rev. E* **47**, 1203 (1993).
[48] S. Asahina, M. Sorai, A. Fukuda, H. Takezoe, K. Furukawa, K. Terashima, Y. Suzuki, and I. Kawamura, *Liq. Cryst.* **23**, 339 (1997).
[49] K. Itoh, M. Kabe, K. Miyachi, Y. Takanishi, K. Ishikawa, H. Takezoe, and A. Fukuda, *J. Mater. Chem.* **7**, 407 (1997).
[50] T. Isozaki, T. Fujikawa, H. Takezoe, A. Fukuda, T. Hagiwara, Y. Suzuki, and I. Kawamura, *Jpn. J. Appl. Phys.* **31**, L1435 (1992).
[51] T. Isozaki, T. Fujikawa, H. Takezoe, A. Fukuda, T. Hagiwara, Y. Suzuki, and I. Kawamura, *Phys. Rev. B* **48**, 13439 (1993).
[52] T. Isozaki, H. Takezoe, A. Fukuda, Y. Suzuki, and I. Kawamura, *J. Mater. Chem.* **4**, 237 (1994).
[53] T. Isozaki, K. Ishikawa, H. Takezoe, and A. Fukuda, *Ferroelectrics* **147**, 121 (1993).
[54] A. Fukuda, Y. Takanishi, T. Isozaki, K. Ishikawa, and H. Takezoe, *J. Mater. Chem.* **4**, 997 (1994).
[55] P. Bak and R. Bruinsma, *Phys. Rev. Lett.* **49**, 249 (1982).
[56] R. Bruinsma and P. Bak, *Phys. Rev. B* **27**, 5824 (1983).
[57] P. Bak, *Physics Today* **39**, 38 (1986).
[58] M. Yamashita and S. Miyajima, *Ferroelectrics* **148**, 1 (1993).
[59] M. Yamashita, *Mol. Cryst. Liq. Cryst.* **263**, 93 (1995).
[60] M. Yamashita, *Ferroelectrics* **181**, 201 (1996).
[61] M. Yamashita, *J. Phys. Soc. Jpn.* **65**, 2122 (1996).
[62] M. Yamashita, *J. Phys. Soc. Jpn.* **65**, 2904 (1996).
[63] T. Koda and H. Kimura, *J. Phys. Soc. Jpn.* **64**, 3787 (1995).
[64] H. Orihara and Y. Ishibashi, *Jpn. J. Appl. Phys.* **29**, L115 (1990).
[65] H. Sun, H. Orihara, and Y. Ishibashi, *J. Phys. Soc. Jpn.* **62**, 2706 (1993).
[66] B. Zeks, R. Blinc, and M. Cepic, *Ferroelectrics* **122**, 221 (1991).
[67] B. Zeks and M. Cepic, *Liq. Cryst.* **14**, 445 (1993).
[68] V.L. Lorman, A.A. Bulbitch, and P. Toledano, *Phys. Rev. E* **49**, 1367 (1994).
[69] M. Cepic and B. Zeks, *Mol. Cryst. Liq. Cryst.* **263**, 61 (1995).

[70] A. Roy and N.V. Madhusudana, *Europhys. Lett*. **36**, 221 (1996).
[71] V.L. Lorman, *Mol. Cryst. Liq. Cryst.* **262**, 437 (1995).
[72] A. Roy and N.V. Madhusudana, *Europhys. Lett*. **41**, 501 (1998).
[73] P. Mach, R. Pindak, A.-M. Levelut, P. Barois, H.T. Nguyen, C.C. Hunag, and L. Furenlid, *Phys. Rev. Lett.* **81**, 1015 (1998).
[74] J. Li, H. Takezoe, and A. Fukuda, *Jpn. J. Appl. Phys.* **30**, 532 (1991).
[75] K. Miyachi, M. Kabe, K. Ishikawa, H. Takezoe, and A. Fukuda, *Ferroelectrics* **147**, 147 (1993).
[76] T. Akizuki, K. Miyachi, Y. Takanishi, K. Ishikawa, H. Takezoe, and A. Fukuda, *Jpn. J. Appl. Phys.* **38**, 4832 (1999).
[77] T. Isozaki, K. Hiraoka, Y. Takanishi, H. Takezoe, A. Fukuda, Y. Suzuki, and I. Kawamura, *Liq. Cryst.* **12**, 59 (1992).
[78] M. Skarabot, M. Cepic, B. Zeks, R. Blinc, G. Heppke, A.V. Kityk, and I. Musevic, *Phys. Rev. E* **58**, 575 (1998).
[79] K. Hiraoka, Y. Takanishi, K. Skarp, H. Takezoe, and A. Fukuda, *Jpn. J. Appl. Phys.* **30**, L1819 (1991).
[80] C. Bahr, D. Fliegner, C.J. Booth, and J.W. Goodby, *Phys. Rev. E* **51**, 3823 (1995).
[81] V. Laux, N. Isaert, H.T. Nguyen, P. Cluseau, and C. Destrade, *Ferroelectrics* **179**, 25 (1996).
[82] K. Yamada, Y. Takanishi, K. Ishikawa, H. Takezoe, A. Fukuda, and M.A. Osipov, *Phys. Rev. E* **56**, R43 (1997).
[83] A. Rastegar, M. Ochsenbein, I. Musevic, T. Rasing, and G. Heppke, *Ferroelectrics* **212**, 249 (1998).
[84] K. Ema, M. Kanai, H. Yao, Y. Takanishi, and H. Takezoe, *Phys. Rev. E* **61**, 1585 (2000).
[85] S. Inui, N. Iimura, T. Suzuki, H. Iwane, K. Miyachi, Y. Takanishi, and A. Fukuda, *J. Mater. Chem.* **6**, 71 (1996).
[86] A. Fukuda, S.S. Seomun, T. Takahashi, Y. Takanishi, and K. Ishikawa, *Mol. Cryst. Liq. Cryst.* **303**, 379 (1997).
[87] C. Tanaka, T. Fujiyama, T. Maruyama, and S. Nishiyama, *Abst. of 21st Jpn. Liq. Cryst. Conf.* (Sendai), **2C18** (1995).
[88] S.S. Seomun, Y. Takanishi, K. Ishikawa, H. Takezoe, A. Fukuda, C. Tanaka, T. Fujiyama, T. Maruyama, and S. Nishiyama, *Mol. Cryst. Liq. Cryst.* **303**, 181 (1997).
[89] S.S. Seomun, Y. Takanishi, K. Ishikawa, H. Takezoe, and A. Fukuda, *Jpn. J. Appl. Phys.* **36**, 3586 (1997).
[90] S.S. Seomun, T. Gouda, Y. Takanishi, K. Ishikawa, H. Takezoe, and A. Fukuda, *Liq. Cryst.* **26**, 151 (1999).
[91] A.D.L. Chandani, Y. Cui, S.S. Seomun, Y. Takanishi, K. Ishikawa, H. Takezoe, and A. Fukuda, *Liq. Cryst.* **26**, 167 (1999).
[92] B. Park, S.S. Seomun, M. Nakata, M. Takahashi, Y. Takanishi, K. Ishikawa, and H. Takezoe, *Jpn. J. Appl. Phys.* **38**, 1474 (1999).
[93] S.S. Seomun, B. Park, A.D.L. Chandani, D.S. Hermann, Y. Takanishi, K. Ishikawa, H. Takezoe, and A. Fukuda, *Jpn. J. Appl. Phys.* **37**, L691 (1998).
[94] B. Park, M. Nakata, S.S. Seomun, Y. Takanishi, K. Ishikawa, and H. Takezoe, *Phys. Rev. E* **59**, R3815 (1999).
[95] S.-W. Choi, Y. Kinoshita, B. Park, H. Takezoe, T. Niori, and J. Watanabe, *Jpn. J. Appl. Phys.* **37**, 3408 (1998).
[96] K. Okano, *Jpn. J. Appl. Phys.* **25**, L846 (1986).

[97] M. Nakagawa and T. Akahane, *J. Phys. Soc. Jpn.* **55**, 1516 (1986).
[98] Y. Ouchi, H. Takezoe, and A. Fukuda, *Jpn. J. Appl. Phys.* **26**, 1 (1987).
[99] E. Gorecka, D. Pociecha, M. Glogarova, and J. Mieczkowski, *Phys. Rev. Lett.* **81**, 2946 (1998).
[100] S. Tanaka and M. Yamashita, *Jpn. J. Appl. Phys.* **38**, L139 (1999).
[101] M. Johno, K. Itoh, J. Lee, Y. Ouchi, H. Takezoe, A. Fukuda, and T. Kitazume, *Jpn. J. Appl. Phys.* **29**, L107 (1990).
[102] Y. Yamada, K. Mori, N. Yamamoto, H. Hayashi, K. Nakamura, M. Yamawaki, H. Orihara, and Y. Ishibashi, *Jpn. J. Appl. Phys.* **28**, L1606 (1989).
[103] A.D.L. Chandani, Y. Cui, S.S. Seomun, Y. Takanishi, K. Ishikawa, H. Takezoe, and A. Fukuda, *Mol. Cryst. Liq. Cryst.* **322**, 337 (1998).

As for the molecular orientation structures of the SmCγ* and AF phases discussed on p. 273, recent detailed ellipsometry measurements succeeded in modeling the distorted structures that are distorted from the Ising model and clock model (P.M. Johnson, D.A. Olson, S. Pankratz, T. Nguyen, J. Goodby, M. Hird, and C.C. Huang, *Phys. Rev. Lett.* **84**, 4870 (2000)) and are essentially the same as a distorted Ising model [76].